



All Theses and Dissertations

---

2018-12-01

# Investigation of an IsoTruss Structure as a Compliant Member Used in Bending and Torsion

Jens Garret Jacobson  
*Brigham Young University*

Follow this and additional works at: <https://scholarsarchive.byu.edu/etd>



Part of the [Mechanical Engineering Commons](#)

---

## BYU ScholarsArchive Citation

Jacobson, Jens Garret, "Investigation of an IsoTruss Structure as a Compliant Member Used in Bending and Torsion" (2018). *All Theses and Dissertations*. 7033.

<https://scholarsarchive.byu.edu/etd/7033>

This Thesis is brought to you for free and open access by BYU ScholarsArchive. It has been accepted for inclusion in All Theses and Dissertations by an authorized administrator of BYU ScholarsArchive. For more information, please contact [scholarsarchive@byu.edu](mailto:scholarsarchive@byu.edu), [ellen\\_amatangelo@byu.edu](mailto:ellen_amatangelo@byu.edu).

Investigation of an IsoTruss<sup>®</sup> Structure as a Compliant Member

Used in Bending and Torsion

Jens Garret Jacobson

A thesis submitted to the faculty of  
Brigham Young University  
in partial fulfillment of the requirements for the degree of

Master of Science

Carl D. Sorensen, Chair  
David W. Jensen  
Eric R. Homer

Department of Mechanical Engineering  
Brigham Young University

Copyright © 2018 Jens Garret Jacobson

All Rights Reserved

## ABSTRACT

### Investigation of an IsoTruss<sup>®</sup> Structure as a Compliant Member Used in Bending and Torsion

Jens Garret Jacobson  
Department of Mechanical Engineering, BYU  
Master of Science

An investigation of IsoTruss structures in bending and torsion was conducted. A model was developed in ANSYS APDL where bay length and longitudinal member to helical member cross sectional area ratio could be varied while holding the diameter constant. The model was validated using previously reported values from analytical models and empirical data. The model was used to make predictions of a specific geometry that was manufactured, tested and compared against the model. 12 specimens were built and tested. In flexure, empirical data had a percent error with respect to the model ranging from 10.9 to 65.4% with one outlier at 94.1%. In torsion, the empirical data had a percent error with respect to the model ranging from 0.4 to 34%. The test data exhibited similar trends compared to the model. An IsoTruss structure built to maximize torsional rigidity should have a diameter and bay length such that its helical angle is between 55 and 60 degrees. The inclusion of longitudinal members has a negligible impact on rigidity. Flexural rigidity is maximized with longitudinal members and with a minimal helical angle, placing helical members more in the direction of the longitudinal members. In order to minimize flexural rigidity, the longitudinal members should be removed from the design and the helical member angle should be maximized up to 80 degrees.

Keywords: composite structure, composite design, truss structure, torsion, bending, compliant structure

## ACKNOWLEDGMENTS

First and foremost, I would like to acknowledge my wife, daughter, and newborn son, they supported me, provided motivation, and helped me through the struggles that I faced on a regular basis. I want to thank my advisor, Dr. Sorensen, for the patience that he demonstrated with my questions and in offering his assistance. Thank you to my parents and my parents-in-law who offered their support and prayers for myself and my family. I am grateful for the committee members that have helped along in this process, Dr. Jensen for his deep knowledge base with IsoTruss structures and Dr. Homer for coming on to the committee later in the process.

In addition to the many people involved on a consistent basis, there are many people that helped through different stages. Namely, Casey Tanner, Nick Hawkins, Kevin Cole, Spencer Klakring, Austin Johnson, Kendall Seymour, and Dr. George.

## TABLE OF CONTENTS

<b>LIST OF TABLES</b> . . . . .	<b>vi</b>
<b>LIST OF FIGURES</b> . . . . .	<b>vii</b>
<b>Chapter 1 Introduction</b> . . . . .	<b>1</b>
1.1 Applications With and Without Longitudinal Members . . . . .	1
1.2 Description of IsoTruss Structures . . . . .	1
1.3 Previous Research . . . . .	3
1.4 Research Objectives and Plan . . . . .	5
<b>Chapter 2 Model Development</b> . . . . .	<b>6</b>
2.1 Finite Element Model . . . . .	6
2.1.1 Material Properties . . . . .	7
2.1.2 Geometry . . . . .	7
2.1.3 Boundary Conditions and Loads . . . . .	8
2.2 Comparison with Previous Models . . . . .	8
<b>Chapter 3 Manufacturing and Test Method</b> . . . . .	<b>12</b>
3.1 Specimen Manufacturing . . . . .	12
3.1.1 Mandrel Design . . . . .	12
3.1.2 Mandrel Preparation . . . . .	13
3.1.3 Winding Procedure . . . . .	14
3.1.4 Consolidation Method . . . . .	14
3.1.5 Cure Cycle . . . . .	15
3.1.6 Quality Assessment . . . . .	16
3.1.7 Model Changes . . . . .	19
3.2 Testing Procedure . . . . .	21
3.2.1 Bending Test Apparatus . . . . .	21
3.2.2 Torsion Test Apparatus . . . . .	23
<b>Chapter 4 Results</b> . . . . .	<b>24</b>
4.1 Bending Predictions . . . . .	24
4.2 Bending Test Data . . . . .	26
4.2.1 Flexural Rigidity Dependent on Position . . . . .	27
4.3 Torsion Predictions . . . . .	31

4.4	Torsion Test Data . . . . .	32
<b>Chapter 5</b>	<b>Discussion . . . . .</b>	<b>35</b>
5.1	General Trends . . . . .	35
5.2	Tooling Geometry . . . . .	36
5.3	Curved Longitudinal Members . . . . .	37
5.4	Joint Stiffness . . . . .	37
<b>Chapter 6</b>	<b>Conclusion . . . . .</b>	<b>39</b>
6.1	Recommendations for Future Research . . . . .	40
	<b>REFERENCES . . . . .</b>	<b>42</b>
<b>Appendix A</b>	<b>Manufacturing Documentation . . . . .</b>	<b>43</b>
A.1	Material Data Sheet . . . . .	43
A.2	Mandrel Drawings . . . . .	45
A.3	Cure Temperature Graphs . . . . .	55
A.4	Bending Fixture Drawings . . . . .	58
A.5	Torsion Fixture Drawings . . . . .	64
<b>Appendix B</b>	<b>Raw Data Plots from Testing . . . . .</b>	<b>68</b>
B.1	Raw Data Graphs with Trend Lines . . . . .	68
B.1.1	Torsion . . . . .	68
<b>Appendix C</b>	<b>Finite Element Analysis Batch File . . . . .</b>	<b>72</b>
<b>Appendix D</b>	<b>Derivation of Deflection of a Simply Supported Beam with Eccentric Load . . . . .</b>	<b>82</b>

## LIST OF TABLES

2.1	Material Properties for HexTow PV42/850 12K/UF3323-93 with 30.63% resin content, composite properties were calculated using rule of mixtures [1]. . . . .	7
2.2	Material Properties used in rigidity comparisons with previous models. . . . .	9
2.3	Nomenclature specific to IsoTruss structures. . . . .	9
2.4	Flexural and Torsional Rigidity comparisons between current model and previous models and empirical data. . . . .	11
3.1	Test Matrix outlining the 6 different specimen types being tested. . . . .	12
3.2	Winding Procedure (omit the longitudinal tows for the procedure used for samples without longitudinal members). . . . .	14
4.1	Summary table of the recorded flexural rigidity (kip-in <sup>2</sup> ) for each specimen in 6 different positions with the same minor configuration orientation. . . . .	29
4.2	Summary table of the measured and modeled flexural rigidity with percent error. . . . .	30
4.3	Summary table of the slopes and standard error of the regression lines for the various sets of data from torsion testing. The overall length used in combination with a standard 1 degree rotational deflection to calculate torsional rigidity. . . . .	33
4.4	Summary table of the measured and modeled torsional rigidity with percent error. . . . .	34
D.1	Boundary Conditions . . . . .	84

## LIST OF FIGURES

1.1	Universal joint and the replacement compliant joint concept. . . . .	2
1.2	IsoTruss configurations. Figure Source: Winkel [2]. . . . .	2
1.3	Side profile: geometry nomenclature of an inner grid IsoTruss. . . . .	3
1.4	End view: geometry nomenclature of an inner grid IsoTruss. . . . .	3
2.1	Beam188 element. . . . .	6
2.2	End View of FEA model. . . . .	8
3.1	Aluminum pin mandrels used in manufacturing specimens. . . . .	13
3.2	Positurn 4 digital turntable. . . . .	15
3.3	Cure cycle for specimens 9 and 10, representative of the cure cycle for all specimens. . . . .	16
3.4	Manufacturing deviations of consolidation. . . . .	17
3.5	Manufacturing deviations of crown sections. . . . .	17
3.6	The ideal path of the helical member compared to the member affected by the radius of the peg. . . . .	18
3.7	Detailed view of the longitudinal member as manufactured compared to the intended path. . . . .	18
3.8	Manufacturing deviations of consolidation. . . . .	19
3.9	Axial View: Longitudinal member as manufactured compared to the intended path. . . . .	20
3.10	Side View: Longitudinal member as manufactured compared to the intended path. . . . .	20
3.11	The intended four point bend fixture. . . . .	22
3.12	Two main orientations. . . . .	22
3.13	Torsion test fixture. . . . .	23
4.1	Ideal Predicted Flexural Rigidity v. Helical Angle. . . . .	25
4.2	Ideal Predicted Flexural Rigidity v. Helical:Longitudinal Tow Ratio . . . . .	25
4.3	Predicted Flexural Rigidity v. Helical to Longitudinal Angle, corrected for manufacturing variations. . . . .	26
4.4	Eccentric point load applied to a simply supported beam. . . . .	27
4.5	Load v. Deflection for 6 different positions for sample tested in bending. . . . .	28
4.6	Empirical data superimposed with the as manufactured prediction. . . . .	29
4.7	Enlarged section of Figure 4.1 focusing on configurations without longitudinal members. . . . .	30
4.8	Ideal Predicted Torsional Rigidity v. Helical Angle. . . . .	31



4.9	Predicted Torsional Rigidity v. Helical Angle, corrected for manufacturing variations. . . . .	32
4.10	Empirical Data superimposed with the as manufactured model. . . . .	33
5.1	Representation of the ideal and as manufactured helical shape with applied load. . . . .	36
A.1	Cure cycle for Specimen 2. . . . .	55
A.2	Cure cycle for Specimen 3. . . . .	55
A.3	Cure cycle for Specimen 4. . . . .	56
A.4	Cure cycle for Specimens 5 and 6. . . . .	56
A.5	Cure cycle for Specimens 7 and 8. . . . .	56
A.6	Cure cycle for Specimens 9 and 10. . . . .	57
A.7	Cure cycle for Specimens 11 and 12. . . . .	57
A.8	Cure cycle for Specimen 13. . . . .	57
B.1	Torque v. Rotation for 2 inch Bay Length, 1.0 Longitudinal to Helical Member ratio in torsion test . . . . .	68
B.2	Torque v. Rotation for 2 inch Bay Length, 0.0 Longitudinal to Helical Member ratio in torsion test . . . . .	69
B.3	Torque v. Rotation for 3.5 inch Bay Length, 1.0 Longitudinal to Helical Member ratio in torsion test . . . . .	69
B.4	Torque v. Rotation for 3.5 inch Bay Length, 0.0 Longitudinal to Helical Member ratio in torsion test . . . . .	70
B.5	Torque v. Rotation for 6 inch Bay Length, 1.0 Longitudinal to Helical Member ratio in torsion test . . . . .	70
B.6	Torque v. Rotation for 6 inch Bay Length, 0.0 Longitudinal to Helical Member ratio in torsion test . . . . .	71
D.1	Eccentric load applied to a simply supported beam. . . . .	82

## **CHAPTER 1. INTRODUCTION**

An IsoTruss<sup>®</sup> structure is a cylindrical truss with two types of members, helical and longitudinal. With the removal of the longitudinal members the structure becomes more compliant in bending and attempts have been made to use the structure as a joint to transfer torsion. They are commonly made from advanced composites, including but not limited to epoxy pre-impregnated carbon fiber, fiber glass, aramid, basalt, and other natural fibers. The structure is typically filament wound. Successful applications include telephone poles, construction bracing, concrete column reinforcement, bicycle frames, and drive shafts.

### **1.1 Applications With and Without Longitudinal Members**

In 2016, the BYU SAE Baja team attempted to employ the IsoTruss structure as a drive shaft. This instance was one of the first instances of purposefully building IsoTruss structures without longitudinal members. The initial application was intended to replace the shaft and the joints with a flexurally compliant IsoTruss structure. Essentially replacing the joint seen in Figure 1.1a with the compliant truss in Figure 1.1b. Limitations in understanding the structure's behavior without the longitudinal members prevented further development at that time. The object of this research is to investigate means to design for torsional and flexural rigidity for applications similar to this joint.

### **1.2 Description of IsoTruss Structures**

IsoTruss structures have been made in several configurations: hybrid grid, inner grid, outer grid and a double grid which is a combined inner and outer grid. Hybrid structures use more than one fiber type in the construction of the structure, such as using glass fiber for longitudinal members and carbon fiber for helical members. Figure 1.2 shows single and double grid structures with different terminating features, ending the truss at a set of transition and anti-nodes (crown)



(a) Aluminum and steel universal joint. (b) Prototype 6 node, 2.5 inch compliant joint.

Figure 1.1: Universal joint and the replacement compliant joint concept.

or at a set of nodes. Single grid structures with a crown termination, Figure 1.2c, are the primary focus of this research.

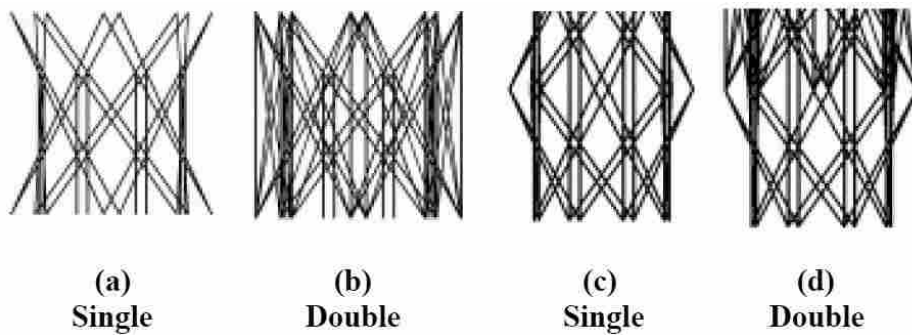


Figure 1.2: IsoTruss configurations. Figure Source: Winkel [2].

With any configuration there are longitudinal members that run the length of the truss and helical members that wrap around the circumference of the truss at an angle to the longitudinal members. The helical members intertwine with other helical members and the longitudinal members at joints, labeled in Figure 1.3 as nodes, transition nodes, and anti-nodes. Nodes are the intersection of the helical members at the maximum diameter for a single grid truss. Transition nodes are where the longitudinal members and helical members intersect. Anti-nodes are the intersection of the helical members at the minor diameter of the truss.

Figure 1.4 shows the end view to further clarify the difference between longitudinal members and helical members. Note the blue points are the ends of the longitudinal members.

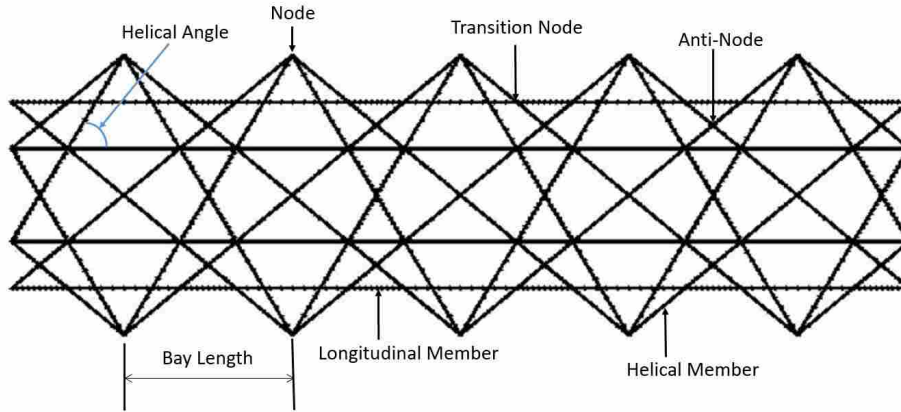


Figure 1.3: Side profile: geometry nomenclature of an inner grid IsoTruss.

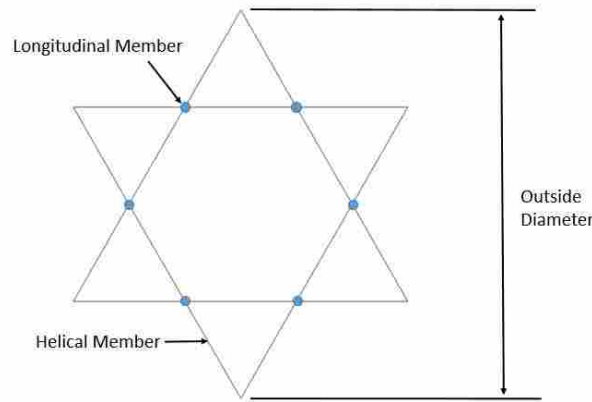


Figure 1.4: End view: geometry nomenclature of an inner grid IsoTruss.

### 1.3 Previous Research

This section outlines the context of the current research. The behavior of IsoTruss structures under bending and torsion loads has been analyzed and tested with a variety of purposes.

Early in the creation of IsoTruss structures, Winkel [2] conducted a parametric investigation of single and double grid trusses with two different end configurations varying the inner and outer longitudinal members, inner and outer helical members, number of nodes, truss diameter, truss length, and bay length. He assumed Timoshenko beam theory neglecting shear deformation in his analysis. This work focused on static loading. Winkel concluded from his analysis that torsion was carried solely by the helical members and axial and bending loads were carried solely in the longitudinal members. Diameter affected torsional and flexural rigidity the most. Winkel

analyzed combined loading of bending and torsion with longitudinal and helical members. Helical member cross sectional area was varied with respect to the longitudinal cross sectional area and it was concluded that helical members do not affect the flexural rigidity but play the major role in torsional rigidity.

Weaver [3], contemporary with Winkel, conducted empirical testing of 23 specimens in compression, tension, torsion, bi-axial tension/torsion, and bi-axial compression/torsion. The specimens were tested to failure and retested to observe the damage tolerance of the redundant structure. The capacity of the specimens was calculated using buckling criteria to predict ultimate load in compression and general material strength for ultimate tensile loads. Measurements during testing were collected using strain gauges attached to individual members. Failure was the primary focus, stiffness was noted but not predicted.

Carroll [4] investigated the residual strength of an IsoTruss structure using finite element methods. Timoshenko beam assumptions with small strains and displacements were applied. A finite element program was written in C++ and validated using ANSYS and ABAQUS. The model validation compared forces in members. Carroll focused on compression, torsion and bending with single grid and hybrid grid IsoTruss structures. Damage was simulated by removing localized helical member sections between nodes in the model. Primary focus was on residual strength, thus stiffness was not predicted or reported.

Brimhall [5] conducted additional experiments exploring the torsional capabilities of the IsoTruss. The primary focus for Brimhall was on the testing method with a secondary focus on the mechanical characteristics of IsoTruss structures in torsion with 3, 6, and 9-tow truss members. Torsional stiffness was not predicted but was reported.

Jensen [6] focused on empirical testing of specimens to determine the flexural behavior of the IsoTruss. Two configurations or orientations were tested, termed the major and minor configuration. The major configuration carried a heavier load. The number of carbon fiber tows in the longitudinal and helical members were also varied; 3, 6, 9, and 18 tows were tested. Comparisons to common aluminum and steel cross sections were made.

Keller [7] conducted an experimental investigation of single and double grid 8-node IsoTruss structures and considered tension, torsion, and flexure. Single grid hybrid specimens were made using carbon fiber and fiber glass and tested in torsion and flexure. Hand calculations were used

to predict the flexural rigidity and Winkel's model was used to calculate a maximum torque and subsequent rotation that were used in predicting torsional rigidity. Integrated cylindrical end caps were evaluated as a functional method of connecting into a structure. An additional process of manufacturing IsoTruss structures was tested using a Solusalt®mandrel. The specimen configurations tested included carbon fiber single grid, carbon fiber double grid, and a hybrid single grid using carbon fiber for the longitudinal members and fiber glass for the helical members.

The research summarized here shows that the behavior with longitudinal and helical members is well understood. There are several areas where it could be strengthened. First, the performance of the structure when longitudinal members are completely removed has not been investigated yet. Next, the behavior in bending has not been analyzed using finite element analysis and tested within the same scope with or without longitudinal members. Finally, the effect that the helical member angle has on flexural and torsional rigidity has not been explicitly analyzed and validated.

#### **1.4 Research Objectives and Plan**

The objective of this research is to develop a set of design rules, ANSYS code and varying plots, that can be utilized in the design of IsoTruss structures in bending and torsion, with and without the incorporation of longitudinal members.

This was accomplished by analyzing the flexural and torsional rigidity of structures while varying the longitudinal cross sectional area and the helical angle using finite element analysis. The model was compared against previous research and empirical data to validate and verify the model. A set of IsoTruss structures was designed, manufactured and tested to confirm the impact of the helical angle, the longitudinal members and the helical members on the flexural and torsional rigidity.

Manufacturing and testing is reported for the benefit of future research and to provide enough detail to replicate any portion as necessary.

## CHAPTER 2. MODEL DEVELOPMENT

This chapter details the assumptions, the element type used, the boundary conditions, and material properties used in the analysis. The model is validated against previous research, both analytical and empirical.

### 2.1 Finite Element Model

The finite element analysis (FEA) model was developed using Beam188 elements in ANSYS APDL which are based on the Timoshenko beam theory [8, 9]. Timoshenko beam theory accounts for shear deformation and can account for bending and shear loads between members through joints. The Beam188 element has 6 degrees of freedom at each joint (see Figure D.1b). This element was selected because this is not a true truss where the members carry only tension and compression loads with pin joints. The members also carry shear loads because moments can be transferred through the joints. The current model does not account for the flexibility attributed to manufacturing imperfection and treats the joint as perfectly rigid. A similar approach was taken by Winkel [2].

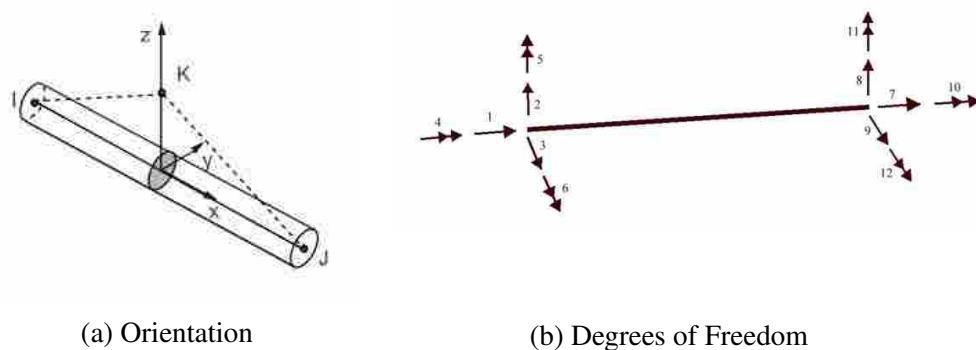


Figure 2.1: Beam188 element.

### 2.1.1 Material Properties

The material used in manufacturing and the properties used in the FEA model are noted in Table 2.1. Due to simplifications from beam theory, Beam188 elements use  $E_x$ ,  $G_{xy}$ , and  $G_{xz}$ .  $G_{xy}$  and  $G_{xz}$  are equivalent in this case due to the fiber running only in a single direction. In assigning material properties, the x-direction runs from I to J in Figure 2.1. The Young's modulus was readily available from the manufacturer or supplier data sheet (see Appendix A.1, the shear modulus was not available and so a similar material was used for the carbon fiber shear modulus [1]. The epoxy shear modulus was calculated based on the isotropic assumption and the Poisson's ratio of 0.35 [1].

Table 2.1: Material Properties for HexTow PV42/850 12K/UF3323-93 with 30.63% resin content, composite properties were calculated using rule of mixtures [1].

	Tensile Strength (Ksi)	Young's Modulus (Mpsi)	Shear Modulus (Mpsi)	Elongation at Failure
Carbon Fiber	884.0	43.0	0.900	2.0%
Resin	9.5	0.410	0.152	5.0%
Prepreg Tow (Spec Sheet)	440.0	25.4	N/A	1.6%
Prepreg Tow (Calculated)	616.1	30.0	0.671	N/A

### 2.1.2 Geometry

The IsoTruss structure can be made in a variety of different configurations. For simplicity, the configuration selected for this investigation was a single inner grid truss that terminates at transition nodes, also termed a crown, see Figure 1.2c. Assumptions made in the model regarding geometry include modeling the truss members with a circular cross section that is constant. All nodes, transition-nodes and anti-nodes have a constant cross section, consistent with the members that intersect at that joint. The intersections in reality have carbon fiber tows that are stacked during subsequent passes in manufacturing, so the joint itself has double or triple the material as manufactured compared to the model. Depending on winding pattern the tows will alternate



direction in a given joint causing gaps if consolidation is not perfect. This is why the modeled joint is more rigid than an as-manufactured joint.

### 2.1.3 Boundary Conditions and Loads

The model assumed a fixed-free, or cantilever, boundary condition where the truss was constrained in all degrees of freedom on the fixed end and a known displacement was applied at the free end. The displacement constraints that were applied were a curvature of 5 degrees about the x-axis for bending and 2.5 degree displacement about the z-axis for torsion. The reaction forces and moments were reported and used in rigidity calculations. The displacements were applied to a central node on the free end where rigid links extend from the central node to the truss ends (see Figure 2.2). Note the beam elements that connect from the end nodes to a center node in red. This node is where the displacements were applied.

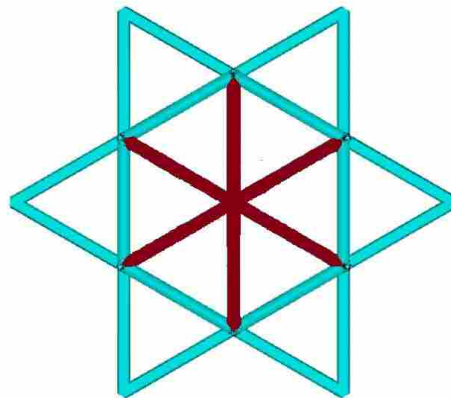


Figure 2.2: End View of FEA model.

## 2.2 Comparison with Previous Models

The model was compared against previous research as well as empirical data from previous testing in order to verify that the current model produces comparable results. The dimensions and material properties used in the current model were as close as could be ascertained from previous documentation (Table 2.2). Table 2.3 shows common nomenclature used to address the different variations and load cases in the remainder of this thesis.

Table 2.2: Material Properties used in rigidity comparisons with previous models.

Model	Young's Modulus (Mpsi)	Shear Modulus (Mpsi)
Winkel	17.0	0.671
Weaver	16.7	0.671
Brimhall	16.7	0.671
Jensen	23.0	0.671
Keller	15.9	0.671

Table 2.3: Nomenclature specific to IsoTruss structures.

Parameter	Description	Variable
Load Case	Bending	B
	Torsion	T
Configuration	6 Node Single Grid Truss	6S
	8 Node Single Grid Truss	8S
	12 Node Single Grid Truss	12S
Dimension	Diameter	d
	Bay Length	b
	Helical tow number	H
	Longitudinal tow number	L
Specimen Number	Subscript for specific specimen	$X_{number}$

Table 2.4 shows the comparison of the model discussed in this chapter with the Winkel and Keller models, as well as the data collected by Weaver, Brimhall, Jensen, and Keller.

Winkel used Timoshenko beam theory assumptions with no allowance for deflection in the elements. The model used in this research used elements based on Timoshenko theory with shear effects, allowing for deflection in an element. Thus Winkel's model should be more stiff and this is reflected in the comparison with Winkel's model surpassing the stiffness in both bending and torsion.

Weaver was about half as stiff compared to the current model. With the model being more rigid than what is actually manufactured. This can be explained by the joints in the model being perfectly rigid while in manufacturing, the joint is less than ideal.

Brimhall nearly matched the model. It was anticipated that the model would be significantly stiffer.

Table 2.4 shows the current model is 25% to 33% less stiff than the empirical data collected by Jensen. This was surprising and counter to the anticipated behavior considering the model's behavior in light of other comparisons.

Keller calculated his theoretical flexural rigidity using the longitudinal modulus of carbon fiber and the area moment of inertia. In considering bending, the helical members were assumed to have little effect and excluded from the inertia calculation. The current model is less stiff compared to the hand calculations which is as anticipated. Keller's reported stiffness for the same configuration is more stiff than his own prediction. I do not have enough information to reach a conclusion whether my model agrees with Keller's reported data.

In torsion, Keller used a finite element program to calculate the maximum member load to cause local buckling and the subsequent torque and deflection were used to calculate the rigidity, GJ. This could explain why his predicted stiffness is less than the current model. Comparing to Keller's empirical torsional rigidity, the model is more stiff as anticipated.

To calculate the error in Table 2.4 it was assumed that the previous research was the standard to compare against.

$$\%Error = \frac{(CurrentModel - PreviousResearch)}{CurrentModel} * 100 \quad (2.1)$$

These comparisons generally confirm that the assumptions made and how the current model as built is accurate. There are a few discrepancies which will not be rectified without further details of how specific tests were conducted or calculations were made.

Table 2.4: Flexural and Torsional Rigidity comparisons between current model and previous models and empirical data.

Thesis	Truss Specification	Data Type	Load Case	Current Model (kip-in <sup>2</sup> )	Previous Research (kip-in <sup>2</sup> )	% Diff.
Winkel	B6S8d7.7b10H10L	Analytical	Bending	1889	2400	-27.1%
Winkel	B12S5d20b10H10L	Analytical	Bending	3510	5000	-42.5%
Jensen	B6S5d2.5b3H3L	Empirical	Bending	298.6	445.0	-49.0%
Jensen	B6S5d2.5b3H3L	Empirical	Bending	601.0	807.0	-34.3%
Keller	B8S2.25d1.5b4H6L	Hand Calc	Bending	199.2	281.0	-41.1%
Keller	B8S2.25d1.5b4H6L	Empirical	Bending	199.2	382.0	-91.8%
Winkel	T6S12d20b10H10L	Analytical	Torsion	2637	6000	-127.5%
Weaver	T6S5d2.5b5H5L	Empirical	Torsion	1975	971.2	50.8%
Brimhall	T6S5d2.5b5H5L	Empirical	Torsion	476.5	482.8	-1.3%
Keller	T8S2.25d1.5b4H6L	Analytical	Torsion	335.9	268.0	20.2%
Keller	T8S2.25d1.5b4H6L	Empirical	Torsion	335.9	138.0	58.9%

## CHAPTER 3. MANUFACTURING AND TEST METHOD

The IsoTruss structure is not easily manufactured. It is beneficial to discuss the process that was used in order to document discrepancies that could impact results as well as offer help for future work.

Table 3.1, shows the test envelope. A 4-inch diameter truss was selected because the test specimens are small enough to test relatively easily and it is easier to consolidate a larger truss. Bay lengths were selected to get a truss with a helical to longitudinal angle of 30, 45 and 60 degrees. The helical members were made with 4 tows, the longitudinal members were either left out completely or were made with 4 tows.

Table 3.1: Test Matrix outlining the 6 different specimen types being tested.

	Value
Diameter (in)	4
Load Cases	Bending, Torsion
Helical Tows	4
Longitudinal Tows	0 or 4
Bay Length (in)	2, 3.5 and 6
Corresponding Helical Angle (degrees)	60, 45 and 30

### 3.1 Specimen Manufacturing

#### 3.1.1 Mandrel Design

The specimens were wound on aluminum pin mandrels, see Figure 3.1. A pin mandrel was selected based on the mandrels that have been used before in research as well in a drive shaft application previous mentioned. The nodal posts were made in 3 different lengths to avoid

redirection of the fiber for the different helical angles caused by the three bay lengths. A 0.25 inch radius was used for where the carbon fiber tow was positioned as to avoid bending the fiber too much or too sharply causing damage to the fiber. 12 screws on either end of the mandrel provided anchor points to start winding from and to allow direction changes. These were labeled with masking tape and numbered to ensure the same pattern was followed and that no helical or longitudinal members were skipped inadvertently.

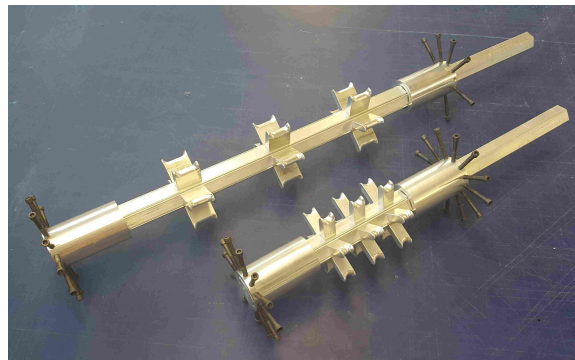


Figure 3.1: Aluminum pin mandrels used in manufacturing specimens.

### 3.1.2 Mandrel Preparation

The mandrels were prepared by knocking off any sharp edges that may come into contact with the carbon fiber tow. Then two coats of Frekote B-15 mold sealer were applied waiting the prescribed 30 minutes between coats. The sealant was cured in an oven at 200°F for two hours. After the sealant was cured, 4 coats of Frekote 700-NC mold release were applied waiting 10 minutes between coats for the release to evaporate. The release was allowed to cure for one hour at room temperature before being used. Every two specimens that were wound a new coat of mold release was applied and cured to ensure removal of specimens with little damage.

### 3.1.3 Winding Procedure

The specimens were wound using a Positurn rotating weld fixture, Figure 3.2. An automated winding apparatus was not available. The Positurn utilizes a foot pedal actuated turn table that rotates up to 10 rpm. This speed was reasonable when placing material by hand.

Typically in winding an IsoTruss structure it is common to completely wrap the end caps at the start of the winding, at the end and in between the completion of a set of helical members or longitudinal members as seems necessary. A set of helical members specifically means a clockwise and counter clockwise winding of the helical members. If the end caps are not built up consistently, there are likely to be considerable air pockets that would introduce stress concentrations. The subsequent winding pattern is listed in Table 3.2.

Table 3.2: Winding Procedure (omit the longitudinal tows for the procedure used for samples without longitudinal members).

Order	Number of Tows
End Cap Layer	2
Helical Tow	1
Longitudinal Tow	1
Helical Tow	1
Longitudinal Tow	1
End Cap Layer	2
Longitudinal Tow	1
Helical Tow	1
Longitudinal Tow	1
Helical Tow	1
End Cap Layer	2

### 3.1.4 Consolidation Method

Pre-impregnated material is commonly used with tooling that can accommodate autoclave pressures and cure cycles to consolidate the fibers and matrix, reducing air pockets in the matrix. The non-traditional geometry of the pin mandrel requires a different approach. Aramid yarn attached to curved needles was used to wrap the truss members and pull the carbon tows together. To



Figure 3.2: Positurn 4 digital turntable.

reduce variability in this process all consolidation was done by the same person using the same pattern at and in between joints. The aramid yarn used was twisted to prevent the yarn from separating and becoming entangled in the mandrel or fraying.

### 3.1.5 Cure Cycle

The resin system used, UF-3323, has a shelf life of 36 months when kept at 0°F. The date of manufacture was November 9, 2016. It was kept out at room temp for about 4 weeks during the manufacturing of specimens. The cure cycle used was a  $\leq 5^\circ\text{F}/\text{minute}$  ramp to 165°F for 2 hours and then a ramp to 300°F for 12 hours. The temperature data was collected using a LabQuest 2 data logger with two type k thermocouples. Figure 3.3 is the cure cycle for specimens 9 and 10 and is representative of all the specimens. The average cure cycle ramp rate was  $\leq 1.9^\circ\text{F}/\text{minute}$ .



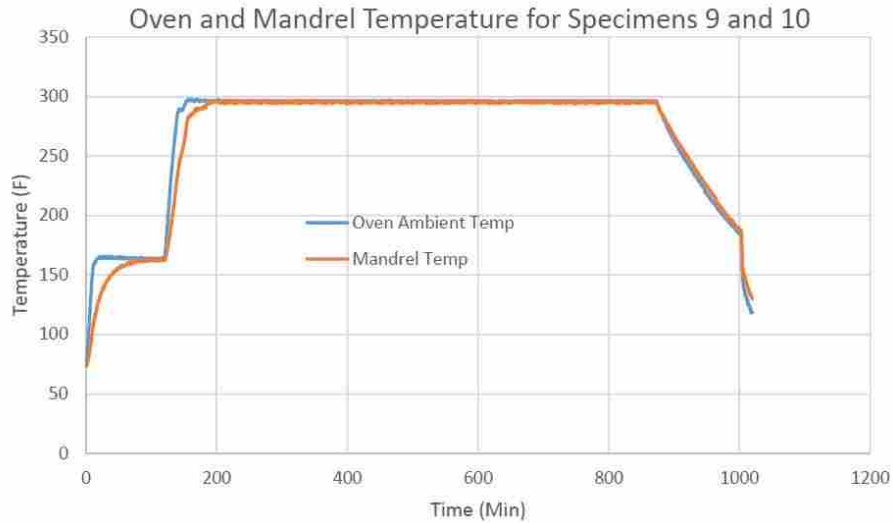


Figure 3.3: Cure cycle for specimens 9 and 10, representative of the cure cycle for all specimens.

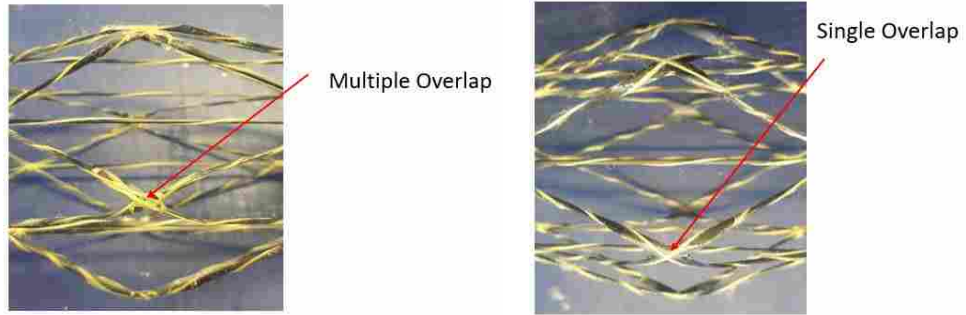
### 3.1.6 Quality Assessment

There are two categories when considering the quality of manufactured samples. The first is sample specific manufacturing deviations and the second is batch deviations or deviations that are consistent within the set of manufactured samples but deviate from the ideal model.

#### Sample Specific Deviations

Specimen 2, in Figure 3.4a, has a slightly different consolidation pattern at the nodes than the other specimens. The aramid fiber was wrapped a few more times than in subsequent trusses. Figure 3.4b shows the typical consolidation method used in the rest of the samples.

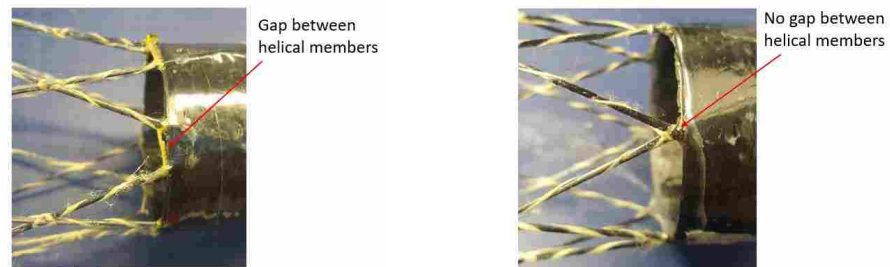
Specimen 2 and 4 have slightly different patterns at where the truss meets the cylindrical end cap, see Figure 3.5a and 3.5c. The helical members are supposed to meet at the same point when coming into the end cap, this indicates that after the last node the angle of the helical member to the longitudinal direction is less than intended. Figures 3.5b and 3.5d show examples of how the crown should terminate to be consistent with the rest of the samples.



(a) Sample 2 Consolidation

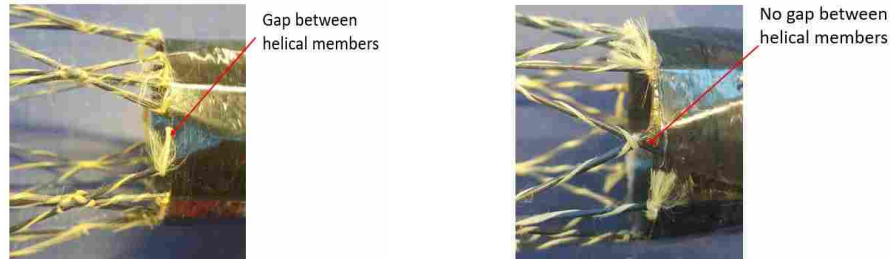
(b) Sample 11 Consolidation

Figure 3.4: Manufacturing deviations of consolidation.



(a) Sample 4 crown

(b) Sample 13 crown



(c) Sample 2 Crown

(d) Sample 11 Crown

Figure 3.5: Manufacturing deviations of crown sections.

### Batch Deviations

It was noted after all specimens were manufactured that there were three deviations from the ideal model and a fourth deviation that was not accounted for. One of these was that the height of the nodal post did not accommodate for the radius used in the aluminum mandrel posts. This meant that the helical member's anti-nodes and transition-nodes were higher than what was intended in the ideal model (See Figure 3.6).

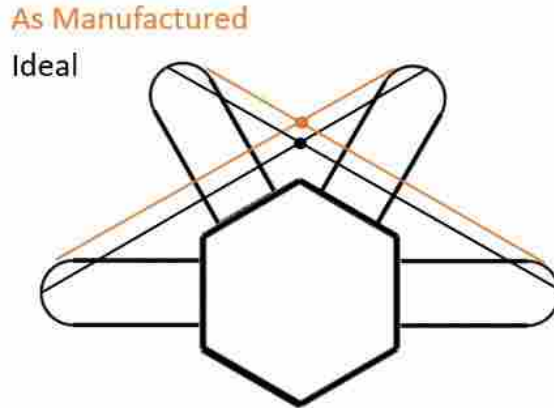


Figure 3.6: The ideal path of the helical member compared to the member affected by the radius of the peg.

The intersections being higher than the model caused the second issue. The issue is that the longitudinal members come off the cylindrical end cap at an angle, thus the longitudinal members are not perfectly straight from end cap to end cap (see Figure 3.7).



Figure 3.7: Detailed view of the longitudinal member as manufactured compared to the intended path.

The third deviation was that there was not a complete crown before the cylindrical end cap, where there should be two sets of transition nodes and a set of anti-nodes. Figure 3.8 shows the difference between the two. During the manufacturing of the specimens the helical members were terminated in line with the nodes rather than in line with the longitudinal members and the transition nodes. These variations from the ideal model were primarily isolated to the cylindrical

end cap interface where the end effects dominate. These variations were corrected for in the model used.

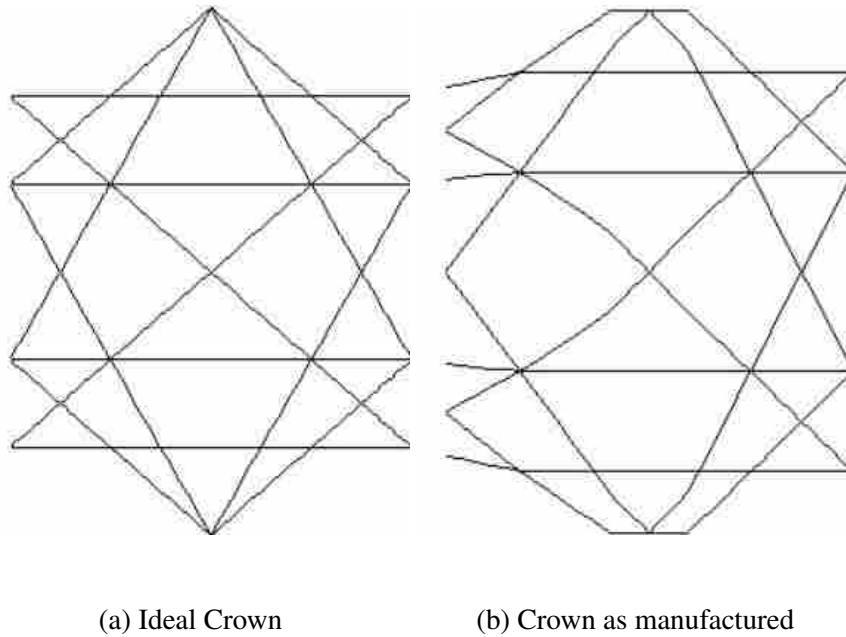


Figure 3.8: Manufacturing deviations of consolidation.

The fourth deviation was that the longitudinal members were also not straight. Figures 3.9 and 3.10 show this issue for sample B6S4d2b4H4L<sub>10</sub>. Two potential reasons for this issue, the first is that the longitudinal members not coming off of the end cap straight might also have caused the longitudinal member to wander. The second is the elongated central portion of the post. This could have caused some wander in the longitudinal direction of where the helical tow comes across the peg. Instead of settling at exact bottom of a curve, there is a flat area leading to issues with accurate location which causes the transition node location to wander. This could not be accounted for in the model because it was not a consistent deviation across all samples.

### 3.1.7 Model Changes

There were three modifications to the model to resolve the geometry issues between the manufactured samples and the model. The first was to correct the transition and anti-node positions. This was done by using a different diameter in the creation of the key points. The next

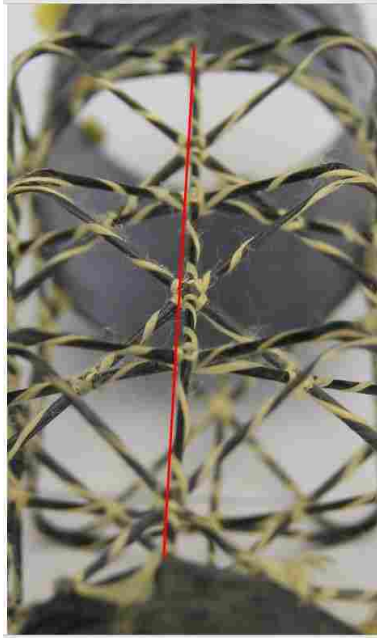


Figure 3.9: Axial View: Longitudinal member as manufactured compared to the intended path.

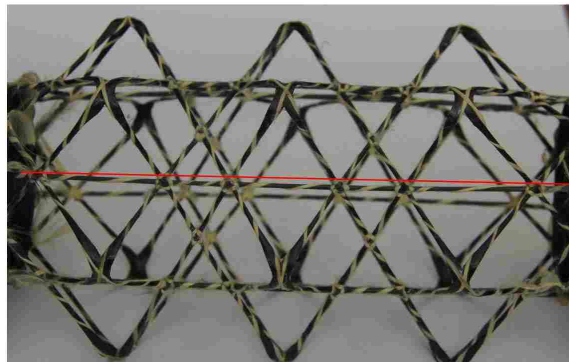


Figure 3.10: Side View: Longitudinal member as manufactured compared to the intended path.

change was to account for the radius of the tooling at the node location. This was done by making key points that were based off the node locations that were offset radially, longitudinally as well as circumferentially so that the key point was essentially at the transition from a straight member to the radius of the tooling. The final modification was to modify the nodes at the crown so that the pattern of manufacturing was mimicked.

## 3.2 Testing Procedure

### 3.2.1 Bending Test Apparatus

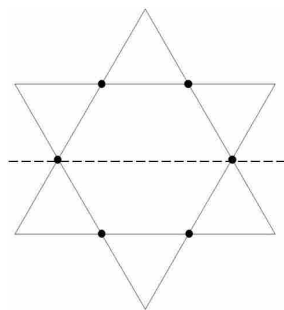
To test the specimens in bending, an adjustable 4 point bending fixture was designed and manufactured as seen in Figure 3.11. Load cells were inserted just above the load applicators. A dial indicator was used to record deflection. The fixture needed to adjust for the different length specimens and be one to two orders more stiff than the test specimens to ensure that the fixture's flexibility did not have a significant impact on the data. The specific drawings used are found in Appendix A. The calculated flexural rigidity,  $EI$ , of the fixture is  $123.7 \times 10^6$  lb-in<sup>2</sup>. The load applicator was modified so a load cell could be attached just above where the load was applied. The dial indicator was placed at the center of the beam. The position of the load cells and the dial indicator also inherently reduces the effect any flexibility in the fixture would have on the accuracy of the measurement.

Ideally, the four point bending test set up would produce a constant moment in the truss portion of the specimen since the truss was supported and loaded at the end caps. During the testing of the specimens, one load cell would contact the specimen before the second load cell. Due to the small deflections that were being applied, the second load cell did not contact the specimen. All data collected was in reality from a three point bending case where the moment and shear were not constant in the truss. Retesting was not deemed necessary because the actual load case was known and the rigidity could be calculated with the data collected, as will be detailed in the next chapter.

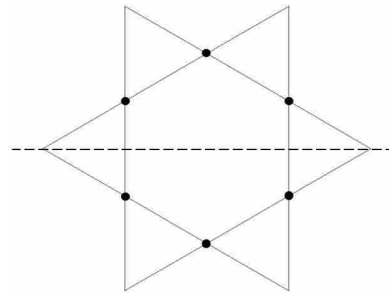
The IsoTruss structure has two distinct orientations and twelve different positions that can be tested in bending. Figure 3.12 shows the two different orientations. These specimens were all tested in the minor configuration, Figure 3.12b, but all six positions were tested to multiple displacements. In each position, the specimen was tested to three different deflections three separate times.



Figure 3.11: The intended four point bend fixture.



(a) Major Configuration



(b) Minor Configuration

Figure 3.12: Two main orientations.



### 3.2.2 Torsion Test Apparatus

To test the specimens in torsion, an insert and clamp fixture was manufactured, see Figure 3.13. All drawings required to manufacture the fixture are in Appendix A. To account for any flexibility inherent in the test fixture a secondary method of measuring displacement was implemented. A system of mirrors and lasers were used to confirm that the rotary position output from the Instron was accurate.



Figure 3.13: Torsion test fixture.



## CHAPTER 4. RESULTS

The model developed in Chapter 2 was used to predict the flexural and torsional rigidity. Plots comparing the rigidity with the helical angle and the longitudinal to helical ratio were made to better understand the behavior in bending and torsion. The helical angle was varied from 25 degrees to 77 degrees. The longitudinal to helical cross-sectional area was varied from zero to one. This chapter reports the predictions made and the results from the flexural and torsion tests conducted.

A total of 12 specimens were tested with a 4-inch diameter, the bay lengths tested were 2 inches, 3.5 inches and 6 inches. Half of the specimens had longitudinal members while the other half had the longitudinal members excluded. All 12 specimens were tested in bending and torsion and were not tested to failure in either instance.

### 4.1 Bending Predictions

The flexural rigidity of the model shown in Figures 4.1 and 4.3 was calculated using Equation 4.1 [10].

$$EI = \frac{ML}{\theta} \quad (4.1)$$

where E is the Young's modulus, I is the area moment of inertia, M is the applied moment reported by model for a given deflection, L is the length of beam, and  $\theta$  is the angle of curvature of the beam, or the angular displacement applied in the model.

Figure 4.1 shows the trends of the ideal model without any modifications for manufacturing variations. This figure shows that as the helical angle is varied, the flexural rigidity remains relatively unchanged. Any impact of the helical member has on flexural rigidity is noticeable at the extreme angles, starting at about 60 degrees.

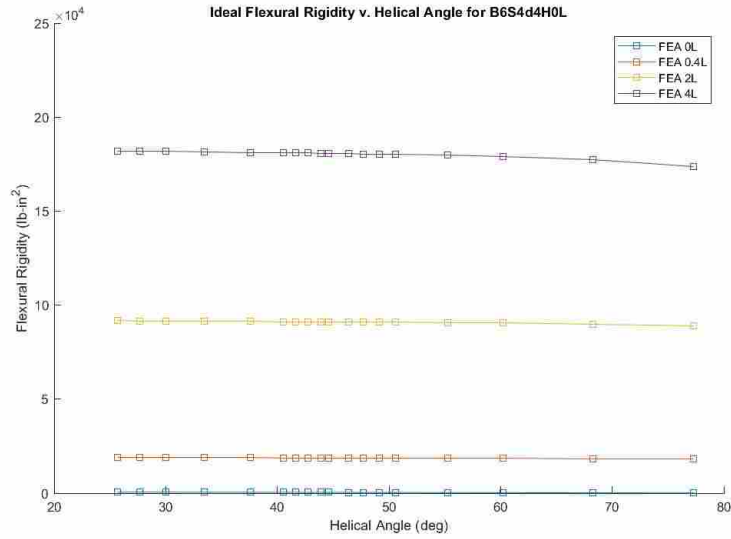


Figure 4.1: Ideal Predicted Flexural Rigidity v. Helical Angle.

Figure 4.2 shows that with zero longitudinal members the flexural rigidity is negligible. The flexural rigidity varies linearly with the longitudinal to helical cross-sectional area ratio. The longitudinal to helical cross-sectional area is based off the number of tows used for the longitudinal members versus the helical with keeping the helical members constant.

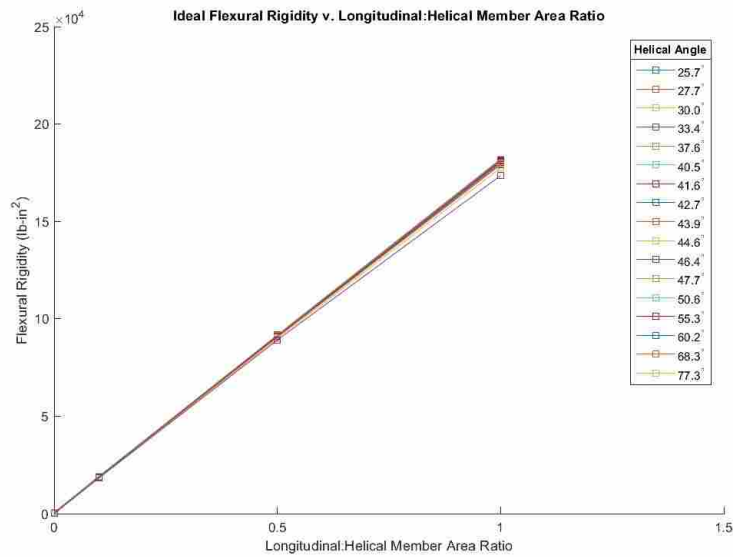


Figure 4.2: Ideal Predicted Flexural Rigidity v. Helical to Longitudinal Cross-sectional Area.

After the manufacturing was completed, the discrepancies noted in Chapter 3 were accounted for in the model. Figure 4.3 shows the change in trends when the longitudinal members are no longer straight and have been shifted out slightly. Due to the overall increase in diameter the overall flexural rigidity is increased by about 16%. The decrease in flexural rigidity as the helical members are not in line with the longitudinal members is more pronounced compared to the ideal geometry.

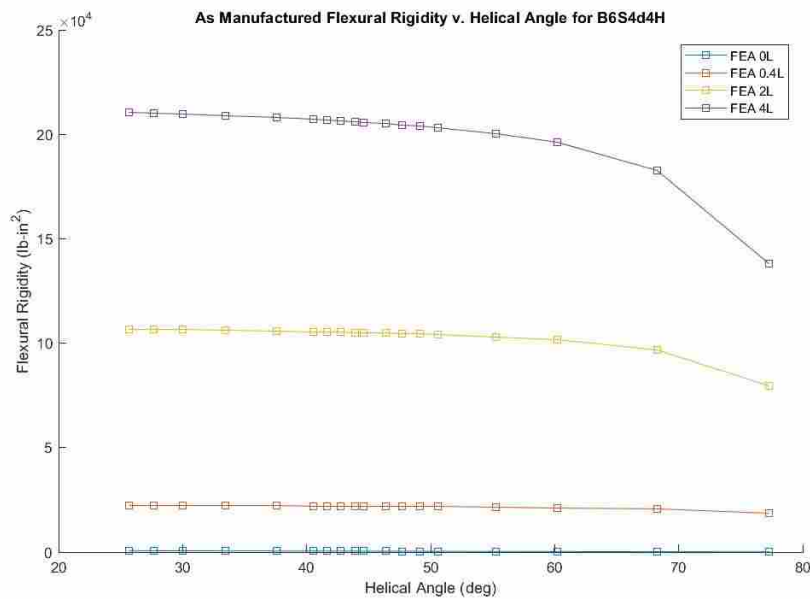


Figure 4.3: Predicted Flexural Rigidity v. Helical to Longitudinal Angle, corrected for manufacturing variations.

## 4.2 Bending Test Data

In the testing of the samples in bending the deflection at the middle of the beam and subsequent load were recorded. The distance from the edge of the near support to the applied load was one inch. The total distance between supports was either 10.6 inches, 15.7 inches or 24 inches for the different bay lengths/helical angles tested. As discussed previously, the load case for the bending tests was a simply supported beam with eccentric point load. A simplified depiction of the load case is seen in Figure 4.4.

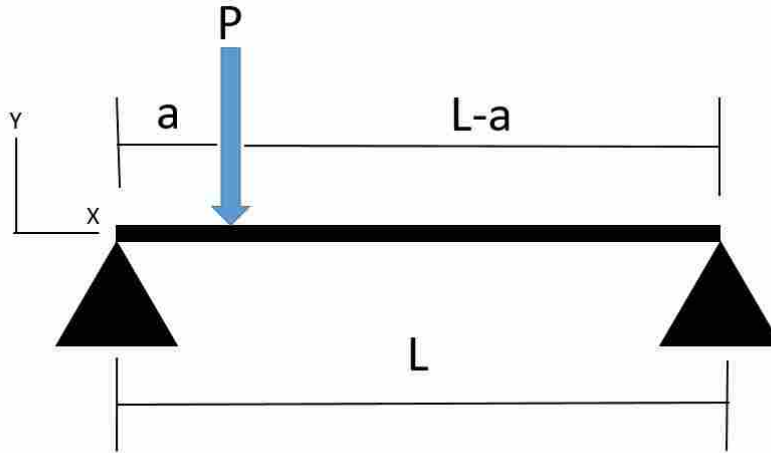


Figure 4.4: Eccentric point load applied to a simply supported beam.

The derivation for the flexural rigidity of a simply supported beam with an eccentric point load is in Appendix D. The equation used to calculate the flexural rigidity is below:

$$EI = -\frac{Pa}{6\delta_{\frac{L}{2}}}(2L-a)(L-a)\left(\frac{L}{2}\right) + \frac{P(L-a)}{6\delta_{\frac{L}{2}}}\left(\frac{L}{2}\right)^3 - \frac{P}{6\delta_{\frac{L}{2}}}\left(\frac{L}{2}-a\right)^3 \quad (4.2)$$

where L is the total length between supports, a is the distance from the near support to the point load, P is the load,  $\delta_{\frac{L}{2}}$  is the displacement at the center of the beam and EI is the flexural rigidity.

#### 4.2.1 Flexural Rigidity Dependent on Position

In conducting the bending tests, it was observed that the rigidity would be significantly impacted by placing the sample in the same orientation for all 6 possible positions in that orientation. Figure 4.5 shows the different load deflection curves for a single specimen that was tested in 6 different positions but the same minor configuration. All specimens were tested in 3-point bending and the test fixtures can be found in Appendix A. The reported stiffness of each specimen is shown in Table 4.1. The recorded slopes and subsequent calculated flexural rigidity in each position is notably different from the next position. Some of the specimens had a reported maximum stiffness as high as 3.34 times its own minimum stiffness.

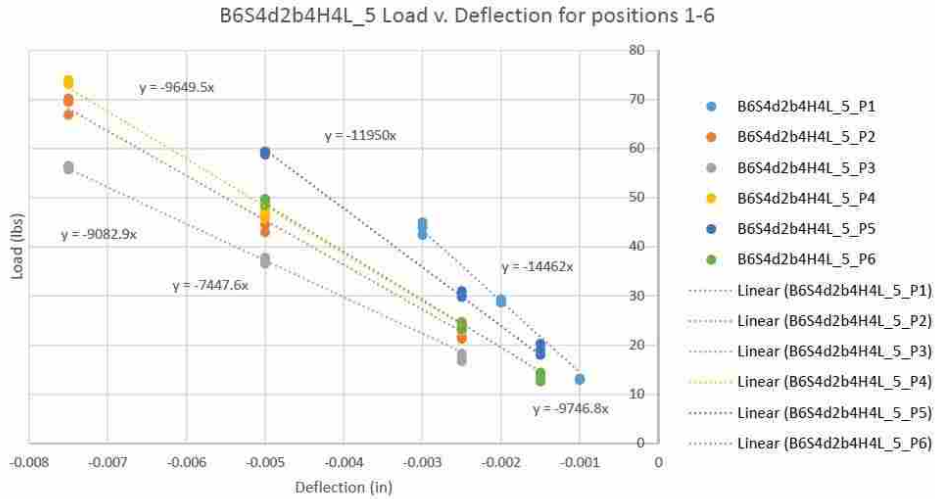


Figure 4.5: Load v. Deflection for 6 different positions for sample tested in bending.

The maximum flexural rigidity for each sample with longitudinal members was used from Table 4.1. This was compared against the designed/manufactured model. The maximum rigidity is closest to what the model represents, which is perfect geometry and consolidation. Any curvature in the manufactured longitudinal member either radially or longitudinally would cause the flexural rigidity to decrease. Comparing the maximum flexural rigidity provides the most ideal tested rigidity to compare against the model. The value compared is the average and standard deviation of the maximum values from the two samples of each geometry. The eliminated values are indicated with a strike through the value.

For the samples without longitudinal members, the average and standard deviation of all the flexural rigidity values for a geometry was used.

From the data, we see the flexural rigidity of an IsoTruss structure with longitudinal members is about two orders of magnitude more rigid than without longitudinal members. The more in line the helical members are with the longitudinal members, the more rigid the structure. From these tests we see an overall increase in flexural rigidity of 70% from the two inch bay length (60 degree helical angle) to the 6 inch bay length (30 degree helical angle).

The flexural rigidity reported in Table 4.1 was compared with the predicted flexural rigidity and plotted against the helical angle in Figures 4.6 and 4.7. The empirical data confirms the general

Table 4.1: Summary table of the recorded flexural rigidity (kip-in<sup>2</sup>) for each specimen in 6 different positions with the same minor configuration orientation.

Specimen	Position						Avg.	Std. Dev.	Coeff. of Var.
	1	2	3	4	5	6			
B6S4d2b4H4L <sub>5</sub>	100.4	63.0	51.7	67.0	82.9	67.6	101.5	1.1	1.1%
B6S4d2b4H4L <sub>10</sub>	64.9	57.6	37.0	45.8	63.6	102.6			
B6S4d2b4H0L <sub>7</sub>	0.384	0.545	0.463	0.650	0.707	0.904	0.626	0.155	24.8%
B6S4d2b4H0L <sub>12</sub>	0.783	0.611	0.534	0.491	0.866	0.571			
B6S4d3.5b4H4L <sub>3</sub>	83.5	109.0	120.2	126.1	166.3	137.1	185.6	19.3	10.4%
B6S4d3.5b4H4L <sub>9</sub>	122.6	116.2	118.3	98.8	205.0	135.5			
B6S4d3.5b4H0L <sub>6</sub>	1.09	0.782	0.662	0.880	0.902	0.835	0.879	0.131	14.9%
B6S4d3.5b4H0L <sub>8</sub>	0.885	0.788	1.13	0.899	0.972	0.728			
B6S4d6b4H4L <sub>2</sub>	161.8	162.5	122.5	155.7	161.8	131.2	172.5	10.0	5.8%
B6S4d6b4H4L <sub>11</sub>	105.0	151.4	182.5	138.8	125.8	141.3			
B6S4d6b4H0L <sub>4</sub>	1.95	1.06	1.86	1.92	3.54	2.55	1.78	0.696	39.1%
B6S4d6b4H0L <sub>13</sub>	2.20	1.23	1.28	1.28	1.16	1.35			

trends that helical members contribute to the flexural rigidity at low helical angles and the flexural rigidity decreases with increasing helical angle.

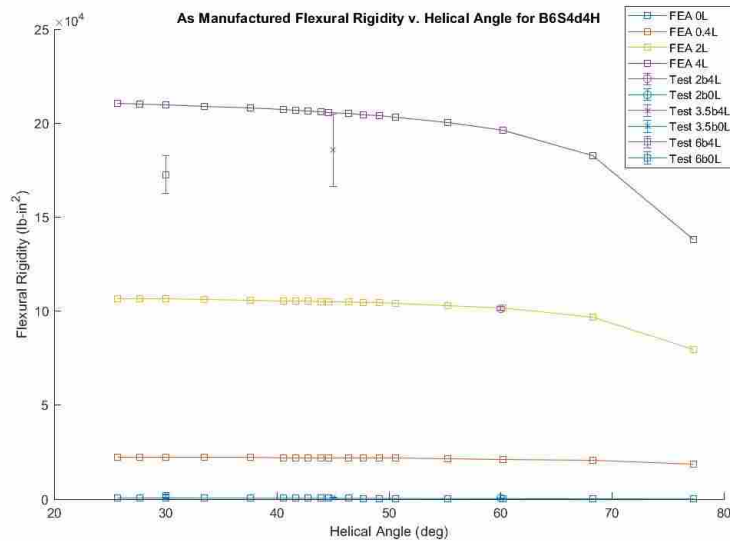


Figure 4.6: Empirical data superimposed with the as manufactured prediction.

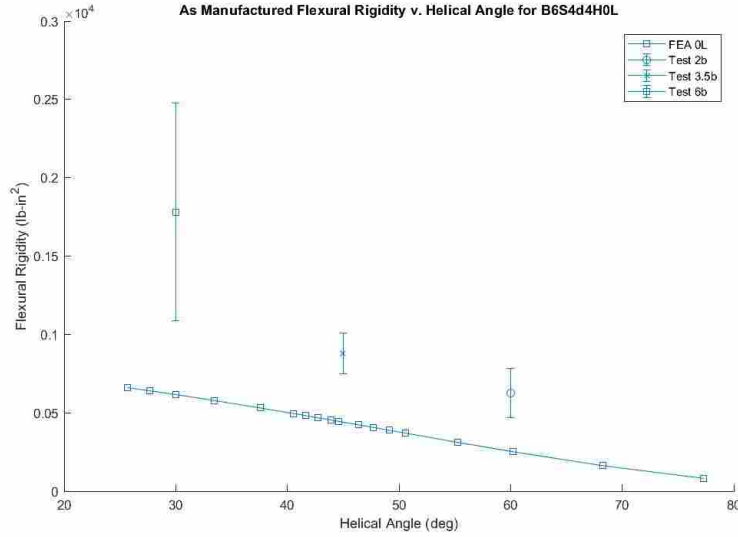


Figure 4.7: Enlarged section of Figure 4.1 focusing on configurations without longitudinal members.

Table 4.2 compares the specific data collected in the tests to the model. The error is calculated as:

$$\%Error = \frac{(ActualValue - PredictedValue)}{ActualValue} * 100 \quad (4.3)$$

The most significant error in Table 4.2 is in the shortest samples with longitudinal members with 93.1% error. The error of the other samples with longitudinal members is 10.9% and 21.3%.

Table 4.2: Summary table of the measured and modeled flexural rigidity with percent error.

Sample	Measured EI (kip in <sup>2</sup> )	Model EI (kip in <sup>2</sup> )	% Error
B6S4d2b4H4L	101.5	196.0	-93.1%
B6S4d2b4H0L	0.626	0.251	59.9%
B6S4d3.5b4H4L	185.6	205.8	-10.9%
B6S4d3.5b4H0L	0.879	0.445	49.4%
B6S4d6b4H4L	172.5	209.2	-21.3%
B6S4d6b4H0L	1.780	0.616	65.4%

### 4.3 Torsion Predictions

The torsional rigidity of the model shown in Figures 4.8 and 4.9 was calculated using Equation 4.4 [10].

$$GJ = \frac{TL}{\phi} \quad (4.4)$$

where  $G$  is the shear modulus,  $J$  is the polar moment of inertia,  $T$  is the applied torque,  $L$  is the length of beam, and  $\phi$  is the angle of twist in radians.

Figure 4.8 shows that the maximum torsional rigidity is achieved at a helical angle of about 55 degrees. The curves that represent the different longitudinal to helical cross-sectional area ratios are all indistinguishable from each other indicating that longitudinal members do not contribute to the torsional rigidity at all.

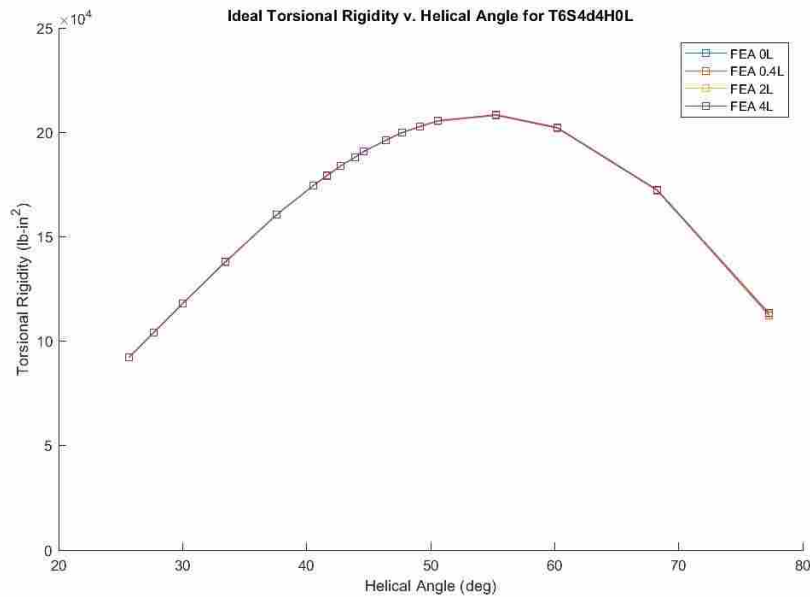


Figure 4.8: Ideal Predicted Torsional Rigidity v. Helical Angle.

The model predictions of torsional rigidity after the manufacturing variations previously discussed were accounted for are shown in Figure 4.9. While the general trend is comparable to



the ideal model in Figure 4.8, the as manufactured model reported values that are about 85% lower when comparing maximum rigidity.

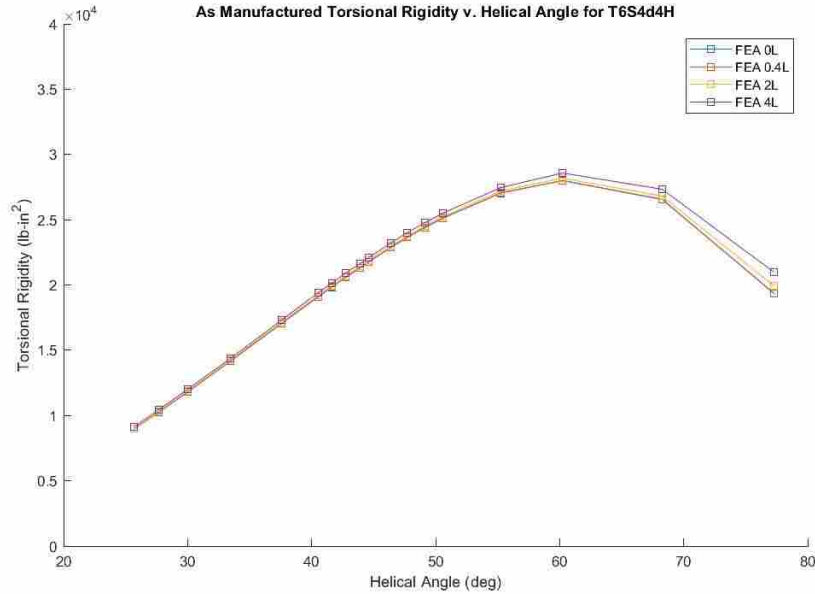


Figure 4.9: Predicted Torsional Rigidity v. Helical Angle, corrected for manufacturing variations.

#### 4.4 Torsion Test Data

In torsion testing the samples, rotational displacement in degrees was recorded using the Instron sensor and confirmed with a laser set up where mirrors were attached to the top and bottom of the truss. A laser was reflected off the mirror onto a wall opposite the fixture and the change in position was measured and the angle of rotation was recorded. The discrepancy between the angle reported by the Instron and the laser measurement was not greater than +/- 0.05 degrees. The torque was recorded using the torsion load sensor standard with the Instron. The same equation, Equation 4.4, was used in calculating the torsional rigidity of the test samples as was used for the model rigidity.

The torsional rigidity is similar with and without longitudinal members as seen in Table 4.3. The rigidity increases as the helical to longitudinal angle increases, reaching a maximum when the

helical is at a 60 degree angle to the longitudinal member or the bay length is 2 inches with a 4 inch diameter.

Table 4.3: Summary table of the slopes and standard error of the regression lines for the various sets of data from torsion testing. The overall length used in combination with a standard 1 degree rotational deflection to calculate torsional rigidity.

Sample	Load/Def (lbs/rad)	Std Error (lbs/rad)	Length (in)	GJ (kip-in <sup>2</sup> )	GJ Error (+/-%)
T6S4d2b4H4L	4308	0.89	10.6	28.4	0.02
T6S4d2b4H0L	5443	1.60	10.6	35.9	0.03
T6S4d3.5b4H4L	2650	4.29	15.7	31.0	0.16
T6S4d3.5b4H0L	2816	1.17	15.7	32.9	0.04
T6S4d6b4H4L	901	1.16	24	18.0	0.13
T6S4d6b4H0L	777	1.29	24	15.5	0.17

The reported torsional rigidity data was superimposed on the plot of the model predictions in Figure 4.10. The same trend exists where the maximum rigidity is at the helical angle of 55-60 degrees.

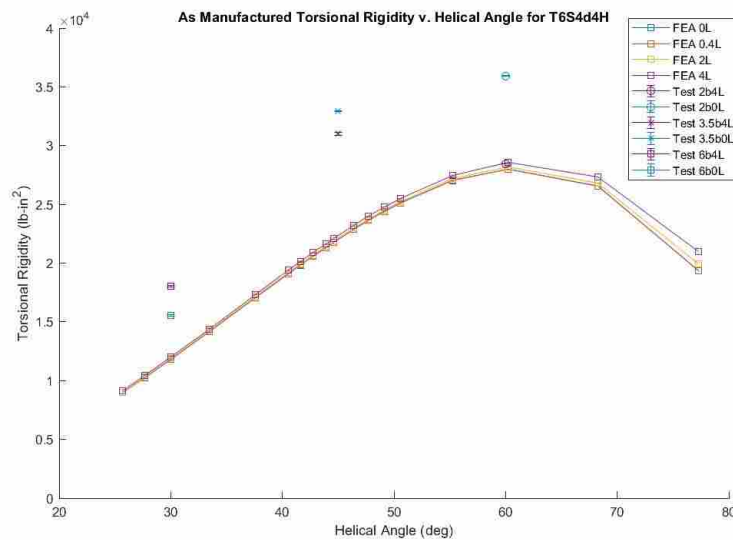


Figure 4.10: Empirical Data superimposed with the as manufactured model.

Table 4.4 compares the error between the model and the test data. In general the model supports the data collected with one outlier at a minimum percent error of 0.4%. The majority of the test data is within 22% to 34% error.

Table 4.4: Summary table of the measured and modeled torsional rigidity with percent error.

Sample	Measured GJ (kip in <sup>2</sup> )	Model GJ (kip in <sup>2</sup> )	% Error
T6S4d2b4H4L	28.4	28.6	-0.41%
T6S4d2b4H0L	35.9	28.0	22.03%
T6S4d3.5b4H4L	31.0	22.1	28.65%
T6S4d3.5b4H0L	32.9	21.8	33.86%
T6S4d6b4H4L	18.0	12.0	33.44%
T6S4d6b4H0L	15.5	11.8	24.03%

## CHAPTER 5. DISCUSSION

This chapter covers the trends seen in the results as well as observations dealing with the joint stiffness, the impact of the helical member angle on rigidity, and the effect of tooling geometry on the rigidity of IsoTruss structures.

### 5.1 General Trends

There are several trends exhibited in both the model and the test data. In the flexural rigidity predicted behavior plot based on the ideal model, Figure 4.1, varying the helical angle did little to impact the flexural rigidity. At extreme angles, the rigidity decreased by 4.4% for a truss with equal number of helical and longitudinal tows, indicating that the flexural rigidity is significantly affected by the longitudinal members and very little effect from helical members. In removing the longitudinal members all together, the flexural rigidity decreases by two orders of magnitude. This empirically confirms observations made by Winkel [2] that longitudinal members carry the majority of a bending load. However, the remaining helical members do contribute to the flexural rigidity. Without the longitudinal members the stiffness of the helical members is enough to affect a design if full compliance in bending is required (Figure 4.7).

In correcting the model for manufacturing variations it was observed that if the longitudinal members are not straight, the contribution of the helical members to flexural rigidity is more significant (Figure 4.3). Carroll [4] explored the residual strength of IsoTruss structures, in that application, if a minimum flexural rigidity is required a shallow helical angle would help. The more in line the helical members are with the longitudinal members, the more flexural rigidity will be maintained in the event of a longitudinal member locally buckling or being damaged.

From Figure 4.8, the torsional rigidity appears to be solely dependent on the helical members. It is maximized when the helical angle is 55-60 degrees from the longitudinal members. When the helical angle is less than 55 degrees the rate of change of the rigidity is less than when

the angle is above 60 degrees. If you wanted to modify your torsional rigidity you would have less drastic change if you modified it below 55 degrees. When longitudinal members are removed, the torsional rigidity is not affected at all.

## 5.2 Tooling Geometry

The tooling was designed with a 0.25-inch radius to minimize the carbon fiber tow being bent around sharp edges and radii. The radius at the node locations impacts the geometry of the helical members. Instead of the helical members being manufactured straight from node to node as is represented in the ideal model, each end of the helical member has a radius. Reference to flexibility in curved beams in tensile loads and buckling loads. Figure 5.1 shows the difference between how an ideal helical member would be loaded in tension and how the manufactured helical would be loaded. The curved helical would be loaded in bending and more compliant compared to a straight member. Similarly with a compressive load applied, the member is curved and therefore easier to deflect (i.e., reduced axial stiffness).

would be to therefore and add i.e., reduced axial stiffness

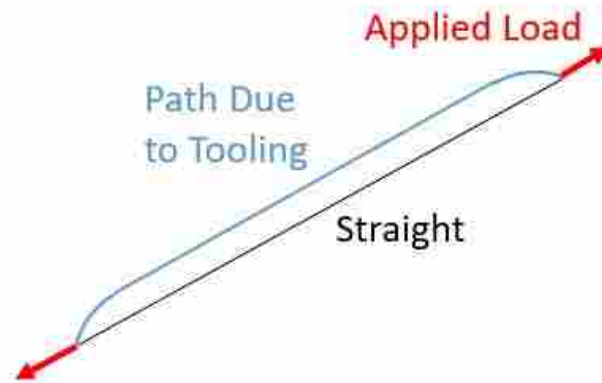


Figure 5.1: Representation of the ideal and as manufactured helical shape with applied load.

The maximum torsional rigidity in the ideal model is 208.4 kip-in<sup>2</sup>. The maximum torsional rigidity in the designed/manufactured model is 28.5 kip-in<sup>2</sup>. There is an 85% decrease in the maximum torsional rigidity for this geometry when accounting for the radius at the nodes.

This significant reduction in torsional rigidity from the ideal model to the as manufactured model is directly from trying to capture the radius at the truss nodes in the model. The test data aligns with the as manufactured model. This suggests that future manufacturing should consider the tooling and the radius used to redirect the helical members as it could have a detrimental effect on the torsional rigidity.

### **5.3 Curved Longitudinal Members**

The drastic step in error of the samples with longitudinal members in Table 4.2 is attributed to the curvature of the longitudinal members. The curvature is more pronounced in shorter bay lengths because any offset between transition nodes would mean a steeper angle. With longer bay lengths, there is more distance so small deviations are less noticeable.

### **5.4 Joint Stiffness**

The intersections of the helical members as well as the intersections of the longitudinal members with the helical members, referred to as transition nodes, anti nodes and nodes, are modeled as a solid, consistent joint. This leads to over predictions of the stiffness. This is seen in the reported flexural rigidity of the samples being lower than the model predictions with longitudinal members. The intersections in reality are inter-stacking tows of carbon fiber that allow for gaps to exist, being weaker when cured than if the intersection were one consistent large tow with no gaps. This phenomena of increased flexibility due to intersection consolidation is not observed in the torsional rigidity plots because the modification to account for the radius at the node makes the model more compliant than the inherent flexibility of the manufactured intersection.

The decrease in flexural rigidity is not as significant as the decrease in torsional rigidity from the ideal model predictions to the as manufactured predictions. This is attributed to the longitudinal members being more accurately represented in the model than the helical members. The effect of how the nodes are modeled impacts the helical members directly.

The effect of the helical members with regards to flexural rigidity is noticeable. When the helical members are more in line with the longitudinal members the flexural rigidity is increased. This off-axis alignment effectively reduces the impact the helical members could have. The helical

members are not nearly as stiff because even a slight offset of carbon fiber from the critical axis, like the offset from a longitudinal member to a helical member, is detrimental to the effective stiffness of a continuous fiber composite [1]. This is straight forward in a plate laminate but the principle is similar in this application. This effect in combination with the reduced stiffness of a manufactured joint result in the flexural rigidity being lower than the ideal and as manufactured predictions for geometries with longitudinal members.

## CHAPTER 6. CONCLUSION

In summary, the objectives of this research were to develop a model that could be used to explore the general trends of IsoTruss behavior with and without longitudinal members with varying helical angles. The results of this investigation could be used to develop fundamental design rules for successful applications of IsoTruss structures in bending and torsion, with or without longitudinal members.

In modeling the truss, I would recommend continuing to include shear deformation effects. The model used in this research included shear deformation, and comparing against previous models, was less rigid. The batch file with modified geometry has been included in Appendix C.

The results show that the model developed provides insight into flexural rigidity trends and predicts trends of torsional rigidity in IsoTruss structures. The longitudinal members in IsoTruss structures contribute the most to flexural rigidity. In the event that longitudinal members are not straight, flexural rigidity is dependent on the helical angle and longitudinal cross-sectional area. Torsional rigidity is solely dependant on the helical members. Removal of the longitudinal members has no impact on the torsional rigidity.

Plots have been developed that give a designer insight into the general behavior of the IsoTruss structure with and without longitudinal members. Several design rules that can be used are:

1. Torsional rigidity is maximized with a helical angle of 55-60 degrees.
2. Torsional rigidity is negatively impacted by the radius of the tooling at the node locations.
3. Flexural compliance is improved with the removal of longitudinal members and a steep helical angle ( $\geq 60$  degrees).
4. Longitudinal members provide no quantifiable contribution to torsional rigidity.



5. Flexural rigidity can be significant enough without longitudinal members to require consideration in low tolerance applications.

Several unanticipated behaviors were observed and noted relating to the manufacturing discrepancies. In bending, IsoTruss structures can have significant variability in their flexural rigidity, even just by rotating the truss by 60 degrees in a 6 node truss. Flexural rigidity is significantly impaired if the longitudinal members are not straight and the helical angle is steep. If the helical members are more in line with the longitudinal members, even if the longitudinal members are not straight the flexural rigidity is not affected as much.

The research conducted should be considered only within the dimensions, materials, manufacturing processes, and ratios investigated.

## **6.1 Recommendations for Future Research**

Through out this research there have been observations of further work that could contribute to the development and effective application of IsoTruss structures. Additional investigations could consider:

1. Modeling the IsoTruss joint specifically, the stacking of tows at joints is not accurately characterized. This would improve the ability to predict torsional rigidity.
2. Investigating the variability of flexural rigidity in different positions to determine if there is a specific manufacturing issue that affects it the most.
3. Quantifying the variability of the different manufacturing methods, potentially by measuring the flexural rigidity in the major and minor configurations and the subsequent repeated positions in those configurations.
4. Comparing the different manufacturing processes by either strength or stiffness.
5. Fatigue strength of an IsoTruss structure without longitudinal members transferring a load between two offset shafts.
6. Comparing stiffness to weight ratio of trusses with different helical angles to see if there is an optimal helical angle from that metric.


7. Axial stiffness with out longitudinal members.

## REFERENCES


- [1] Gibson, R. F., 2012. *Principles of Composite Material Mechanics.*, 3rd ed. CRC Press Taylor & Francis Group, Boca Raton, FL. vi, 7, 38
- [2] Winkel, L. D., 2001. “Parametric Investigation of IsoTruss Geometry Using Linear Finite Element Analysis.” Master’s thesis, Brigham Young University. vii, 2, 3, 6, 35
- [3] Weaver, T. J., 1999. “Mechanical Characterization of a Graphite/Epoxy IsoTruss Subjected to Simple and Biaxial Loads.” Master’s thesis, Brigham Young University. 4
- [4] Carroll, T. S., 2005. “Predicted Residual Strength of Damaged IsoTruss Structures.” Master’s thesis, Brigham Young University. 4, 35
- [5] Brimhall, J., 2000. “Torsional Behavior of a Graphite/Epoxy IsoTruss.” Master’s thesis, Brigham Young University. 4
- [6] Jensen, C. M., 2000. “Flexural Behavior of a Graphite/Epoxy IsoTruss.” Master’s thesis, Brigham Young University. 4
- [7] Keller, B. S., 2002. “Tension, Torsion, and Flexure of an IsoTruss Structure with an Integral Cylindrical End.” Master’s thesis, Brigham Young University. 4
- [8] Labuschagn, A., Rensburg, N. F. V., and van der Merwe, A., 2009. “Comparison of linear beam theories.” *IEEE Transactions on Communications*, **49**, January, pp. 20–30. 6
- [9] ANSYS Beam188 [https://ansyshelp.ansys.com/account/secured?returnurl=/Views/Secured/corp/v191/ans\\_elem/Hlp\\_E\\_BEAM188.html](https://ansyshelp.ansys.com/account/secured?returnurl=/Views/Secured/corp/v191/ans_elem/Hlp_E_BEAM188.html) Accessed: 2018-10-19. 6
- [10] Gere, J. M., and Goodno, B. J., 2012. *Mechanics of Materials.*, 8th ed. 24, 31, 83

## APPENDIX A. MANUFACTURING DOCUMENTATION

### A.1 Material Data Sheet



**HexTow® PV42/850**  
Carbon Fiber



Product Data Sheet

HexTow® PV42/850 carbon fiber is a continuous, high performance, intermediate modulus, PAN based fiber available in 12,000 (12K) filament count tows. This fiber has been surface treated and can be sized to improve its interlaminar shear properties, handling characteristics, and structural properties. It is suggested for use in prepregging, filament winding, braiding, and pultrusion.

The unique properties of HexTow® PV42/850 fiber, such as higher tensile strength and modulus, as well as good shear strength, allow structural designers to achieve both higher safety margins for both stiffness and strength critical applications.

Typical Fiber Properties	U.S. Units	SI Units
Tensile Strength 12K	884 ksi	6,095 MPa
Tensile Modulus (Chord 6000-1000)	43.0 Msi	296 GPa
Ultimate Elongation at Failure 12K	2.0%	2.0%
Density	0.0650 lb/in <sup>3</sup>	1.80 g/cm <sup>3</sup>
Weight/Length 12K	24.7 x 10 <sup>-6</sup> lb/in	0.441 g/m
Approximate Yield 12K	3,372 ft/lb	2.27 m/g
Tow Cross-Sectional Area 12K	3.80 x 10 <sup>-4</sup> in <sup>2</sup>	0.25 mm <sup>2</sup>
Filament Diameter	0.201 mil	5.1 microns
Carbon Content	95.0%	95.0%
Twist	Never Twisted	Never Twisted

Typical 350°F Epoxy Composite Properties (at Room Temperature)	U.S. Units	SI Units	Test Method
0° Tensile Strength	440 ksi	3,034 MPa	ASTM D3039
0° Tensile Modulus	25.4 ksi	175 GPa	
0° Tensile Strain	1.6%	1.6%	
0° Short Beam Shear Strength	17.3 ksi	119 MPa	ASTM D2344
0° Compressive Strength	290 ksi	1,988 MPa	ASTM Mod. D695
0° Open Hole Tensile Strength	67 ksi	460 MPa	ASTM D5766
0° Open Hole Compressive Strength	46 ksi	320 MPa	ASTM D6484
Fiber Volume	60%	60%	

# UF3323 TCR™ Resin

June 2007, Revision 9

TCR Composites offers a unique thermosetting epoxy matrix resin system featuring a **one-year shelf life without refrigeration**. This resin is currently used for tow/roving, unitape, fabric, and braid, and is available for carbon, glass, aramid, and other fibers. Resin content, resin flow during cure, and tack levels can be tailored to suit your process requirements.

## Neat Resin Properties and Applications

Density (g/cc)	Tg (°F/°C) (from G' DMA curve)	Tensile Modulus (ksi/GPa)	Tensile Strength (ksi/MPa)	Elongation at Break (%)	Tg after 24-Hr Water-Boil (°F/°C)	Water Absorption (%)	Available Fiber Form
1.212	240 / 116	410 / 2.83	9.5 / 65.5	5.0	199 / 93	2.5	Tow/Roving, Unitape, Fabric, Braid

## Typical Use

Rocket motor cases, large structures.

## Cure

There are two recommended cure cycles for UF3323 resin. Both will produce similar properties.

1.  $\leq 5^\circ\text{F-per-minute}$  ramp up to  $280^\circ\text{F}$  ( $138^\circ\text{C}$ ), hold for 24 hours,  $< 5^\circ\text{F-per-minute}$  ramp down to at least  $150^\circ\text{F}$  ( $66^\circ\text{C}$ ) before removing from oven.
2.  $\leq 5^\circ\text{F-per-minute}$  ramp up to  $165^\circ\text{F}$  ( $74^\circ\text{C}$ ), hold for 2 hours, ramp up to  $300^\circ\text{F}$  ( $149^\circ\text{C}$ ), hold for 12 hours,  $< 5^\circ\text{F-per-minute}$  ramp down to at least  $150^\circ\text{F}$  ( $66^\circ\text{C}$ ) before removing from oven.

## Storage Requirements

The prepregged materials manufactured from this resin shall remain sealed and stored in the original package. The material is to be stored indoors, out of the weather.

The shelf life is 12 months from the date of manufacture when the maximum storage temperature shall not exceed  $75^\circ\text{F}$  ( $24^\circ\text{C}$ ).

The shelf life is 6 months from the date of manufacture when the maximum storage temperature shall not exceed  $90^\circ\text{F}$  ( $32^\circ\text{C}$ ).

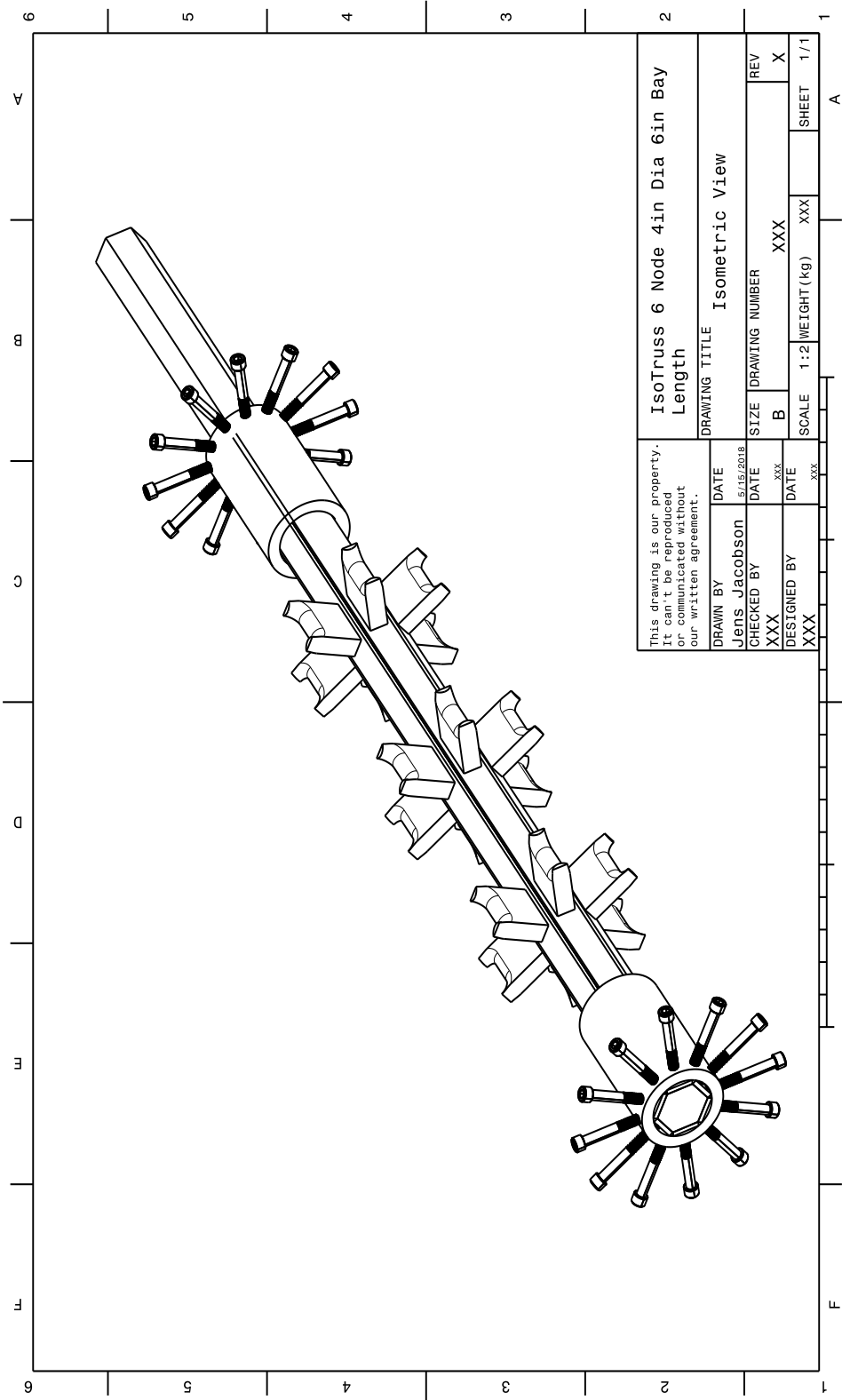
The shelf life is 36 months from the date of manufacture when the maximum storage temperature shall not exceed  $0^\circ\text{F}$  ( $-18^\circ\text{C}$ ), with an additional 6 months at  $<75^\circ\text{F}$  ( $24^\circ\text{C}$ ).

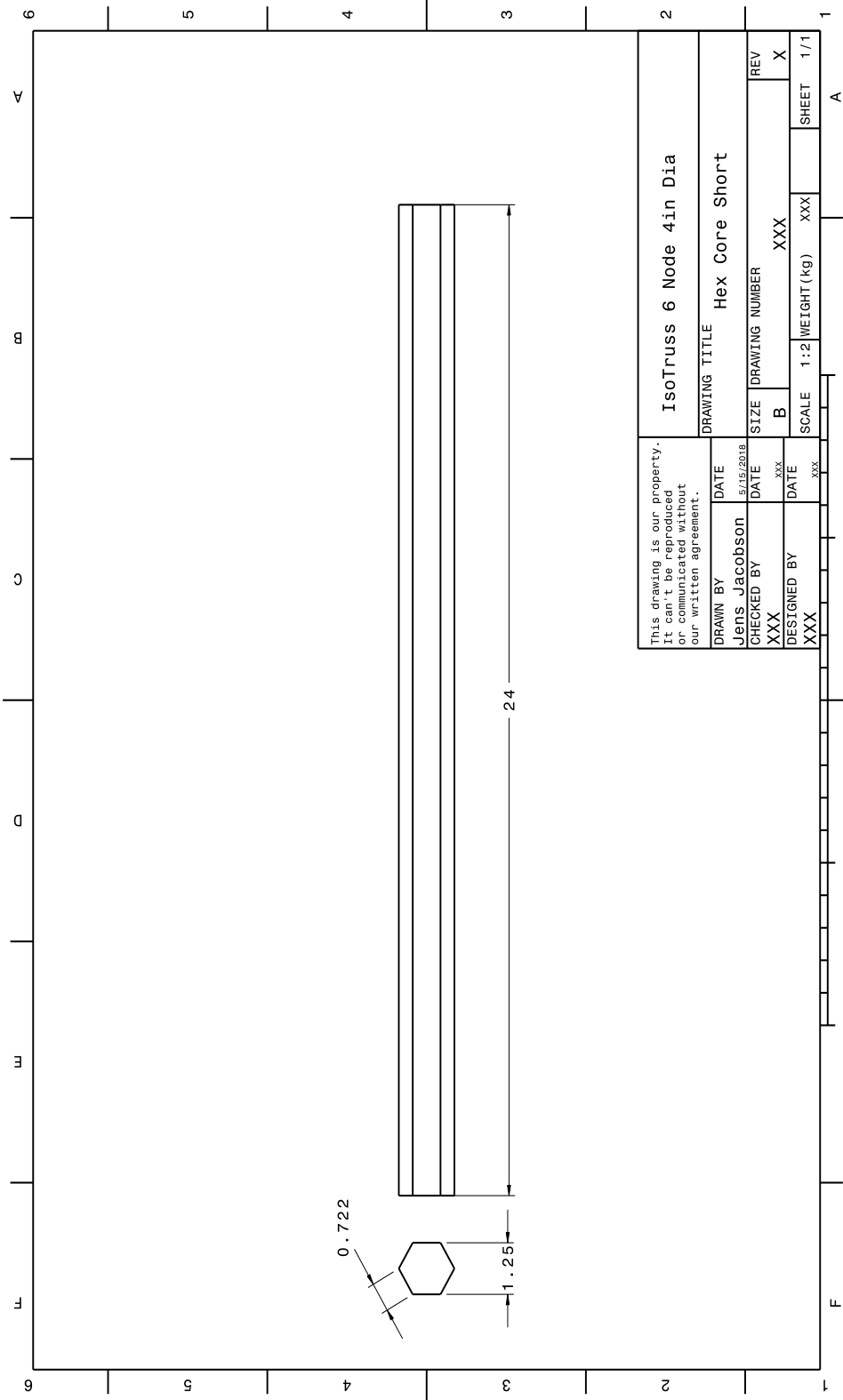
The values here represent expected ranges based on actual test data. Since the values are specimen-preparation- and test-method-dependent, TCR Composites cannot guarantee that these properties will be obtained in all cases. The data should be used as an indication only, since part or component properties are highly equipment- and process-dependent. It is recommended that end users determine the suitability of this material for each application through their own testing and evaluation. TCR™ is a trademark of TCR Composites, Inc.

TCR Composites 219 North 530 West, Ogden, Utah 84404 USA 1- 800-827-3746 1-801-622-3800  
[www.tcrcomposites.com](http://www.tcrcomposites.com)

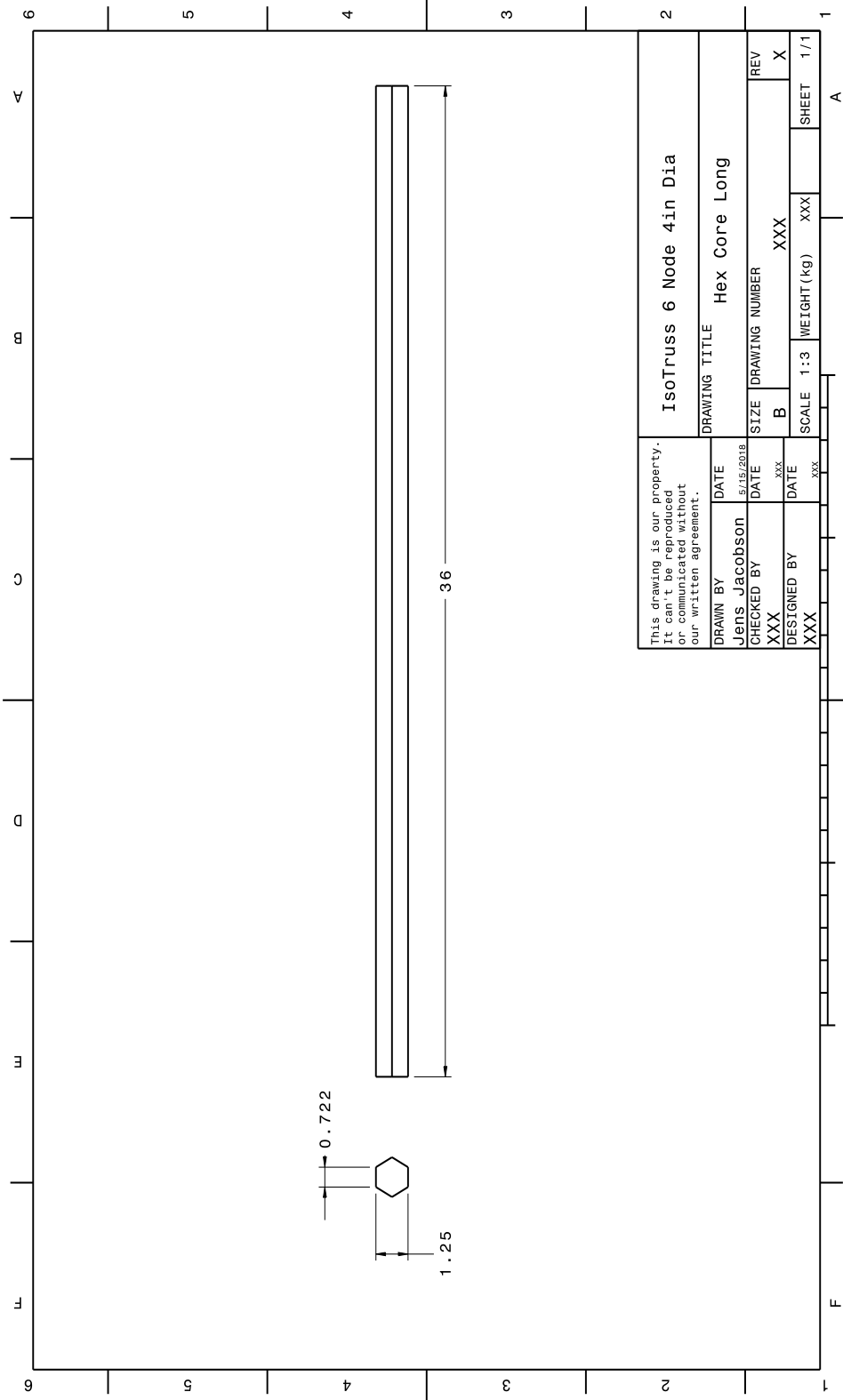
TCR DS-0002/Rev. 9/June 2007

## A.2 Mandrel Drawings



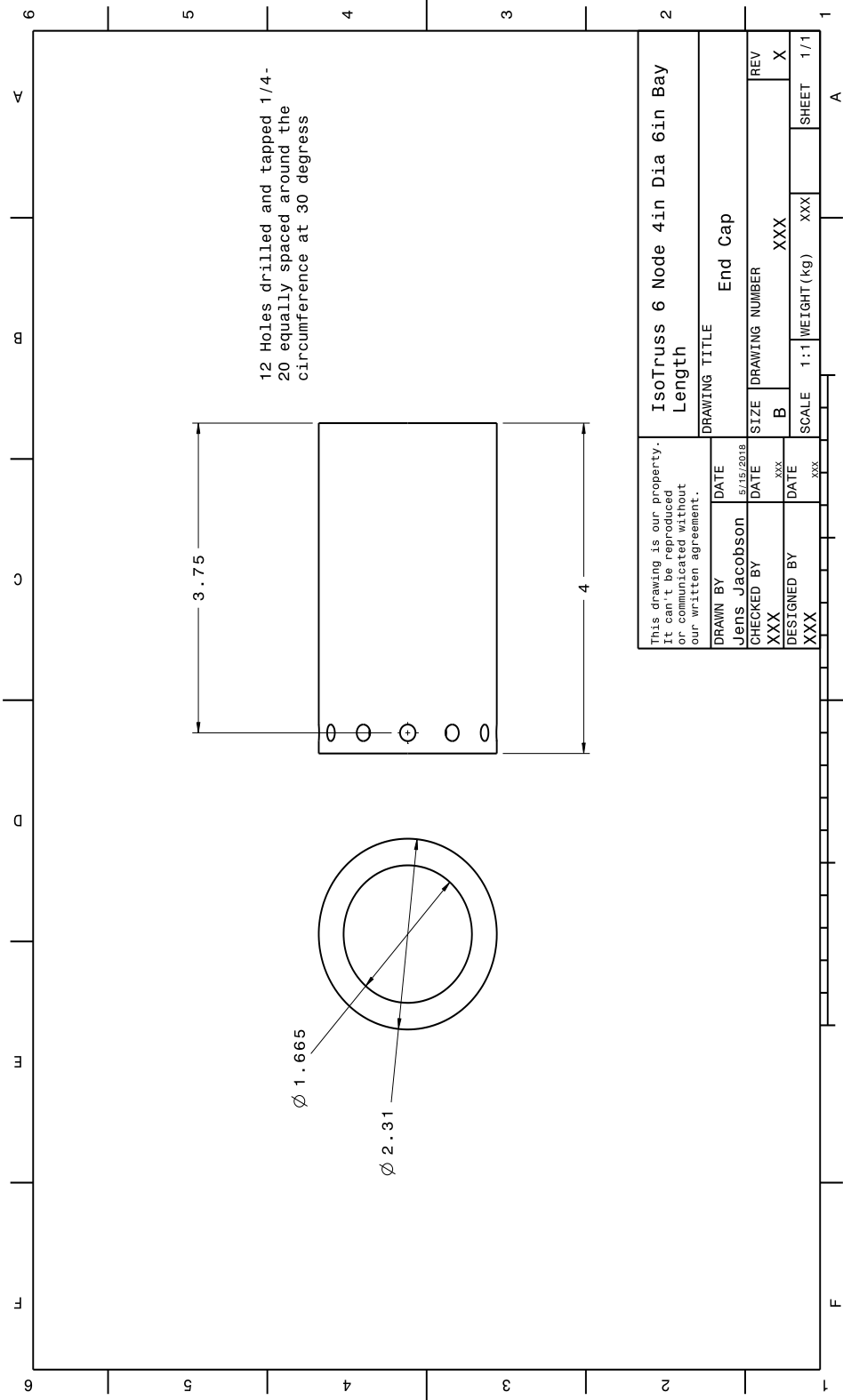


This drawing is our property. It can't be reproduced or communicated without our written agreement.		DRAWING TITLE		ISOTruss 6 Node 4in Dia	
DRAWN BY	DATE	DRAWING NUMBER		REV	
Jens Jacobson	11/15/2018	B		X	
CHECKED BY	DATE	SCALE	1:2	WEIGHT (kg)	XXX
XXX	xxx			SHEET	1/1
DESIGNED BY	DATE				
XXX	xxx				



This drawing is our property. It can't be reproduced or communicated without our written agreement.		DRAWING TITLE		ISOTruss 6 Node 4in Dia	
DRAWN BY	DATE	DRAWING NUMBER		REV	
Jens Jacobson	15/15/2018	B		X	
CHECKED BY	DATE	SCALE	1:3	WEIGHT (kg)	XXX
XXX	xxx			SHEET	1/1
DESIGNED BY	DATE				
XXX	xxx				

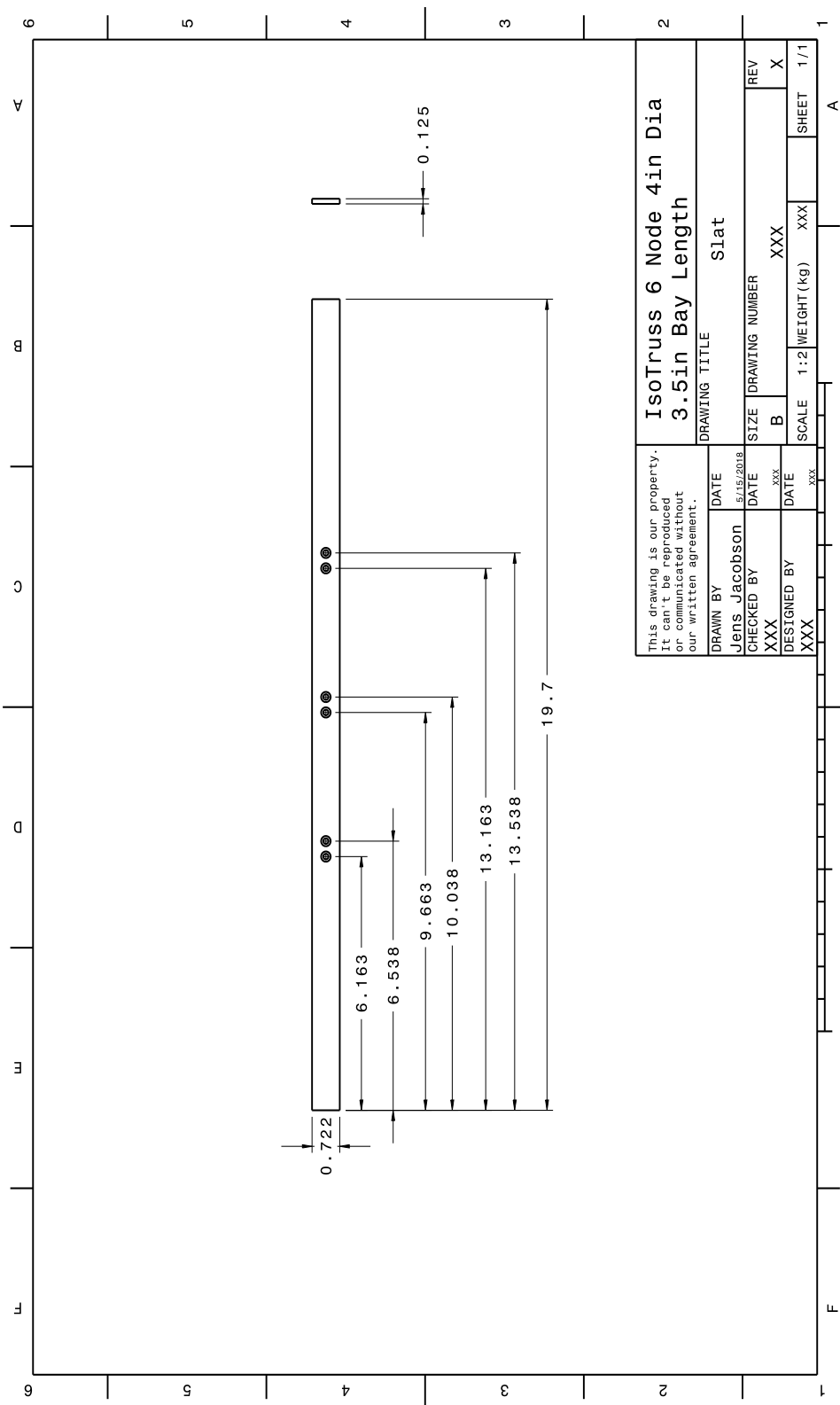




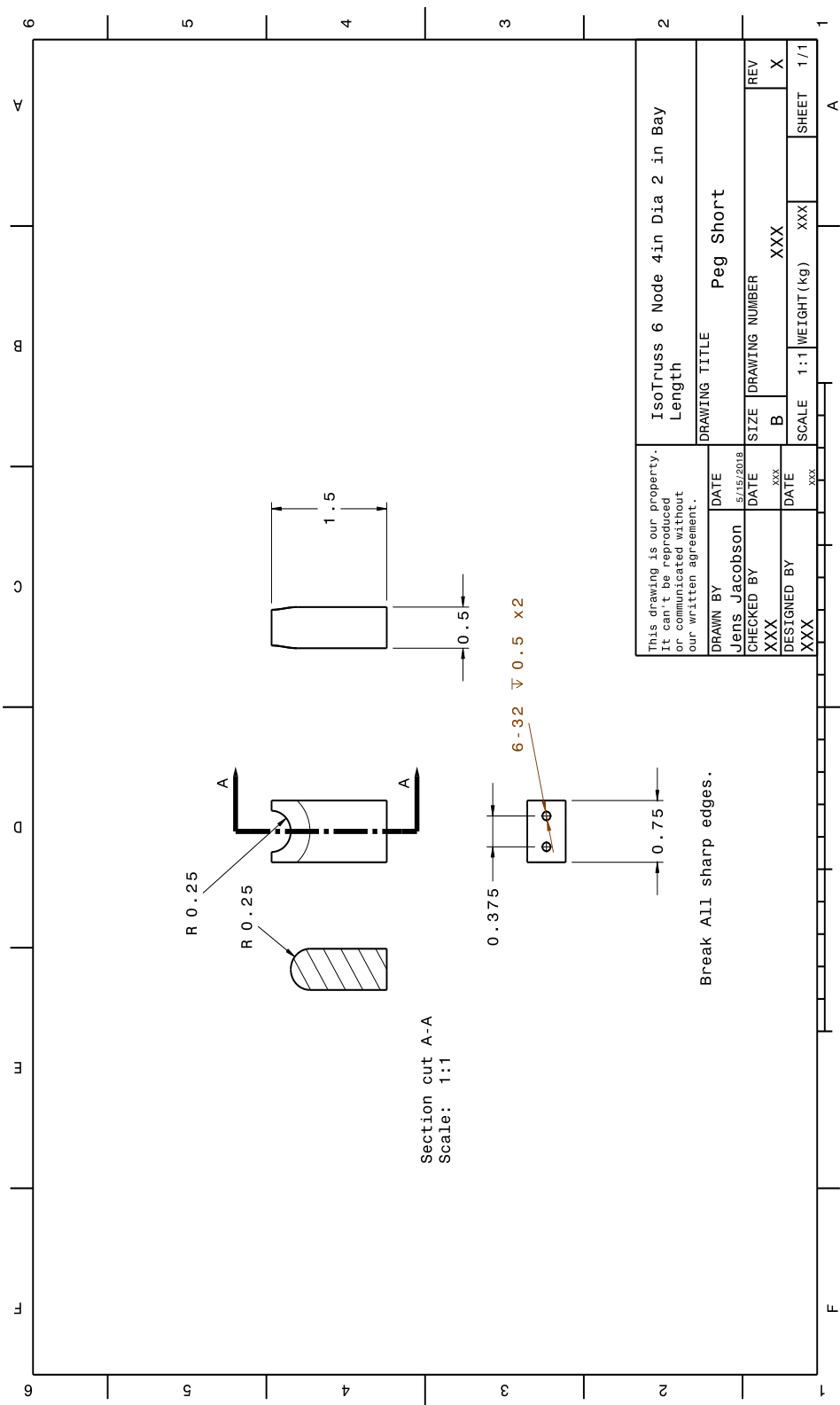




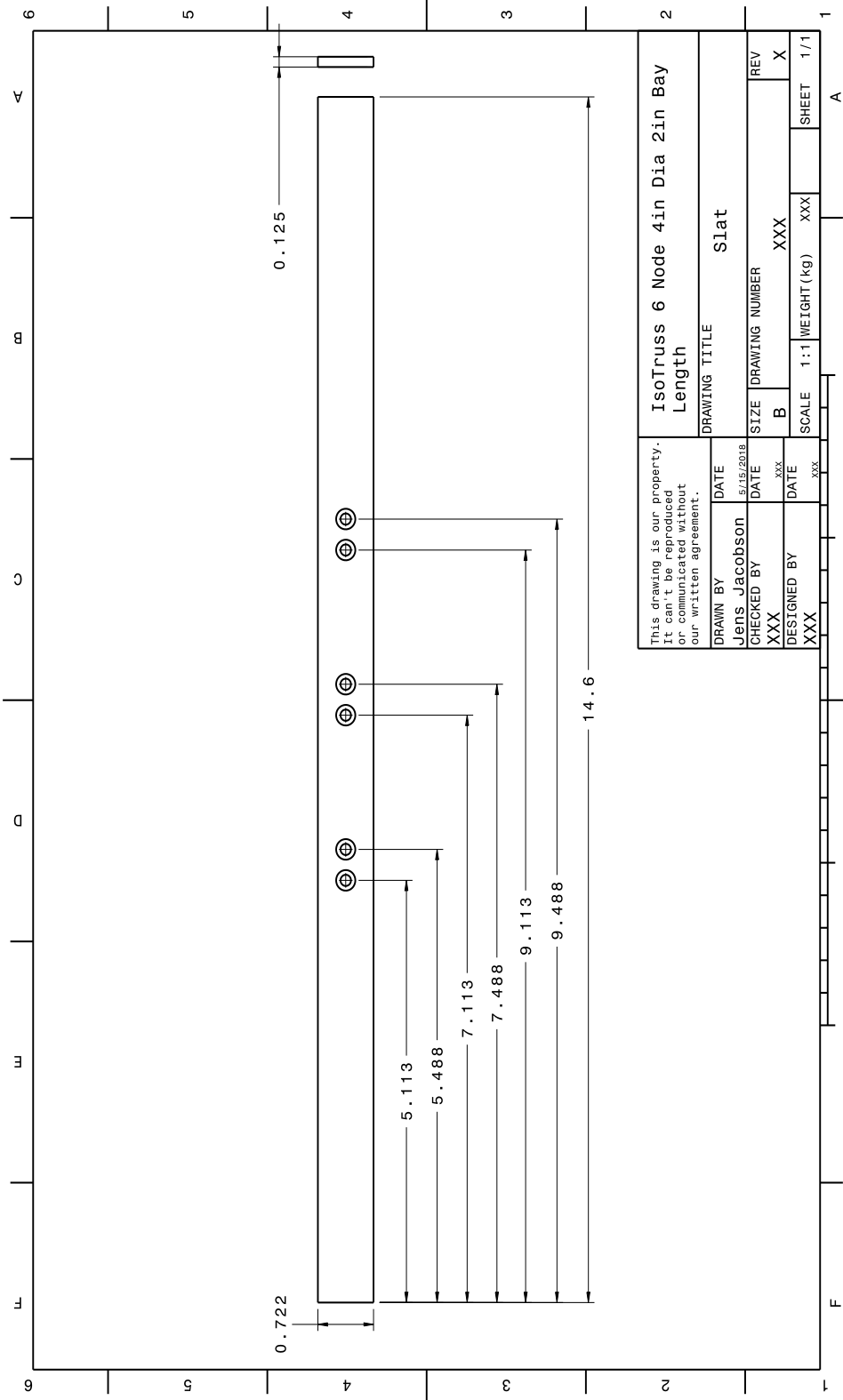




This drawing is our property. It can't be reproduced or communicated without our written agreement.		DRAWING TITLE	
DRAWN BY	DATE	IsoTruss 6 Node 4in Dia 3.5in Bay Length	
Jens Jacobson	11/15/2018	SIZE	DRAWING NUMBER
CHECKED BY	DATE	B	XXX
XXX	xxx	SCALE	1:2 WEIGHT (kg) XXX
DESIGNED BY	DATE	SHEET	1/1
XXX	xxx	A	



This drawing is our property. It can't be reproduced or communicated without our written agreement.		IsoTruss 6 Node 4in Dia 2 in Bay Length	
DRAWING TITLE			
DRAWN BY	DATE	Peg Short	
Jens Jacobson	15/11/2018	SIZE	DRAWING NUMBER
CHECKED BY	DATE	B	XXX
DESIGNED BY	DATE	SCALE	1:1 WEIGHT (kg) XXX
XXX	XXX	SHEET	1/1



This drawing is our property. It can't be reproduced or communicated without our written agreement.		DRAWN BY Jens Jacobson		DATE 15/10/18	IsoTruss 6 Node 4in Dia 2in Bay Length	
CHECKED BY XXX		DATE xxx	DRAWING NUMBER B		REV X	
DESIGNED BY XXX		DATE xxx	SCALE 1:1		WEIGHT (kg) xxx	SHEET 1/1
		DRAWING TITLE Slat		A		

### A.3 Cure Temperature Graphs

Oven and Mandrel Temperature for Specimen 2

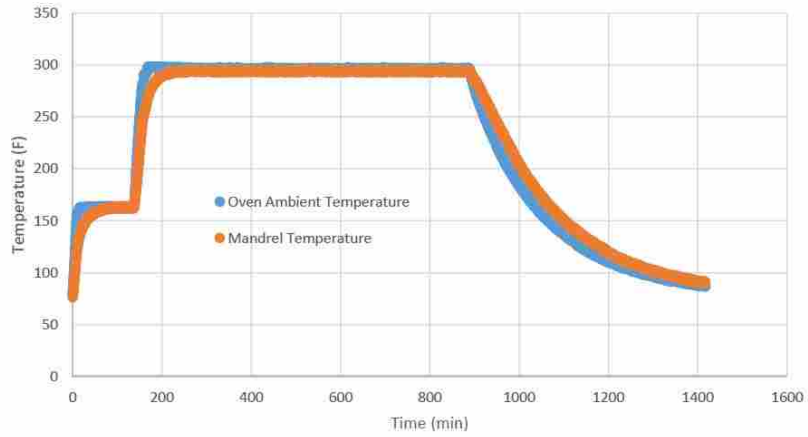


Figure A.1: Cure cycle for Specimen 2.

Oven and Mandrel Temperature for Specimen 3

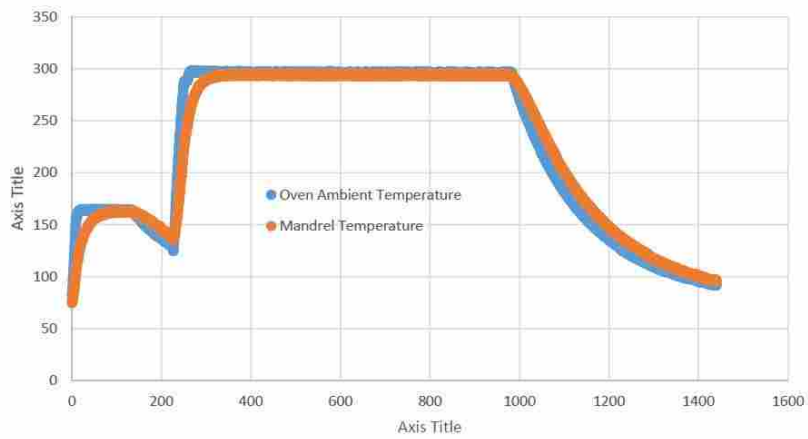


Figure A.2: Cure cycle for Specimen 3.



Oven and Mandrel Temperature for Specimen 4

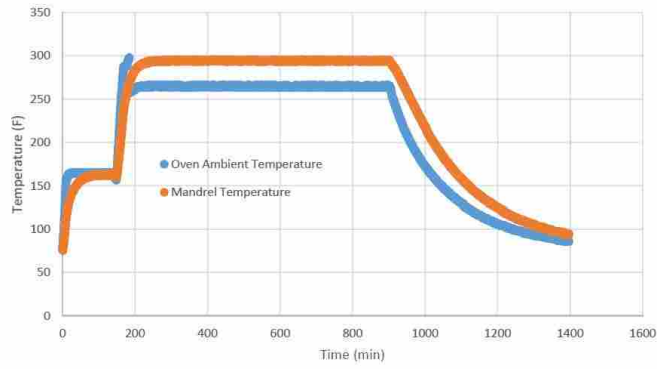


Figure A.3: Cure cycle for Specimen 4.

Oven and Mandrel Temperature for Specimens 5 and 6

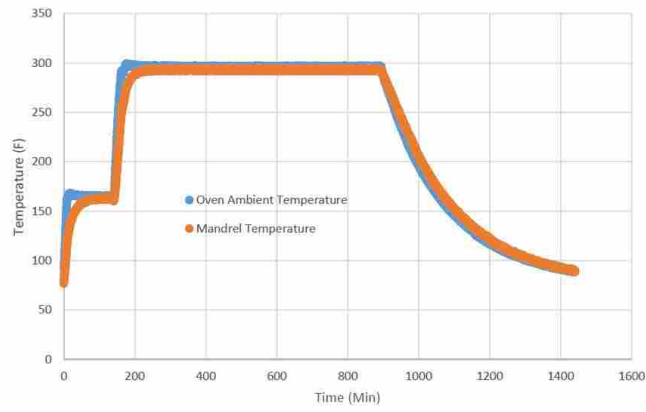


Figure A.4: Cure cycle for Specimens 5 and 6.

Oven and Mandrel Temperature for Specimens 7 and 8

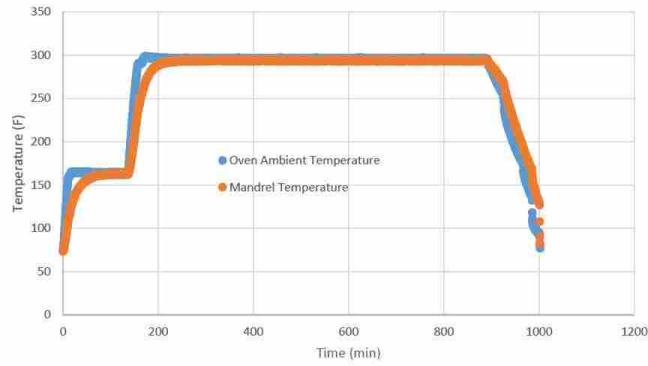


Figure A.5: Cure cycle for Specimens 7 and 8.

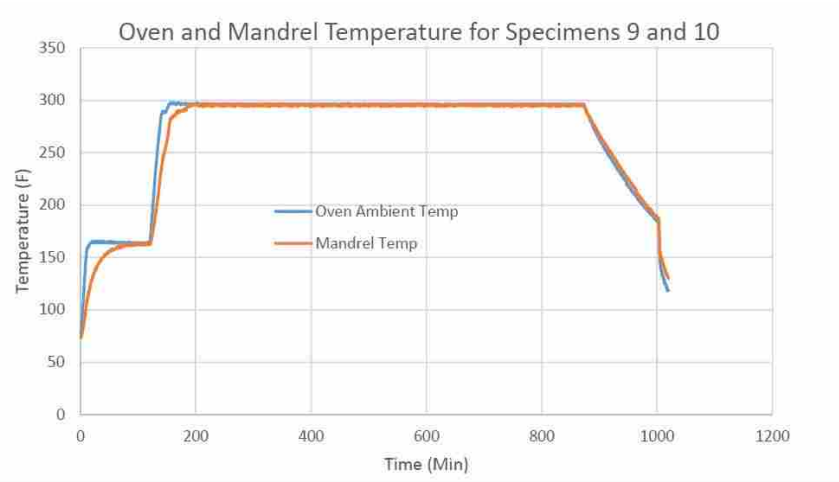


Figure A.6: Cure cycle for Specimens 9 and 10.

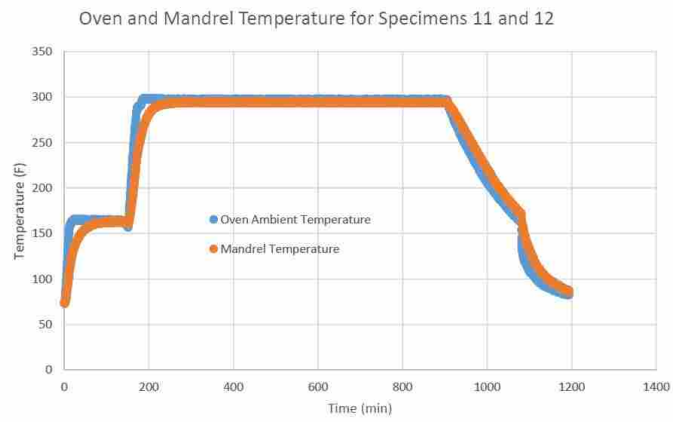


Figure A.7: Cure cycle for Specimens 11 and 12.

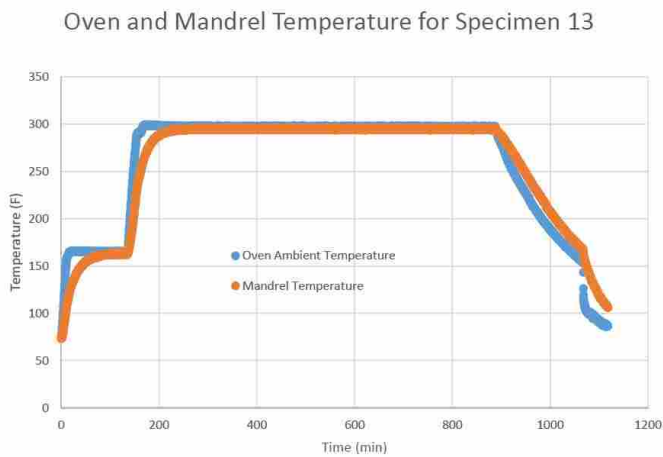
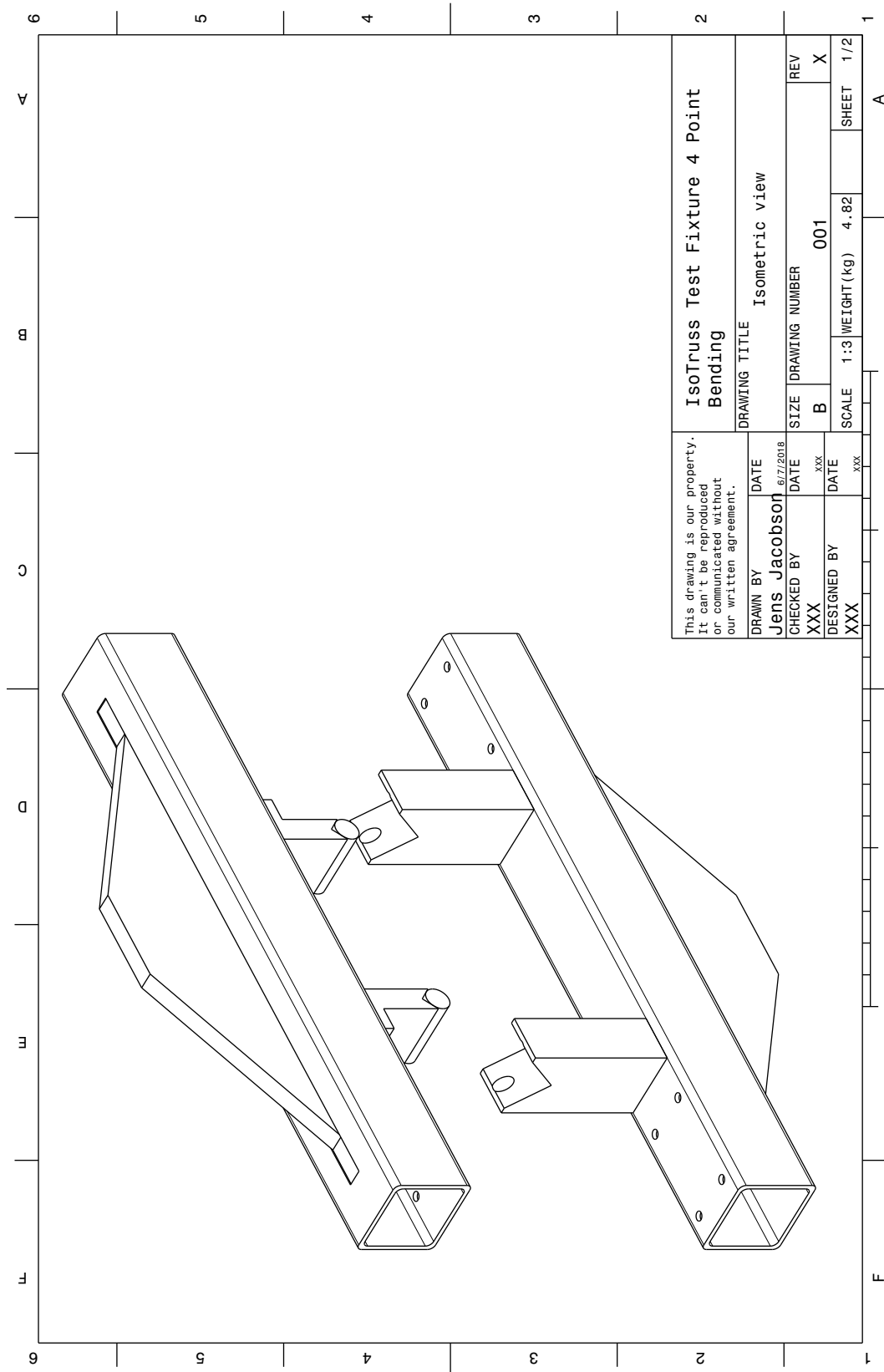
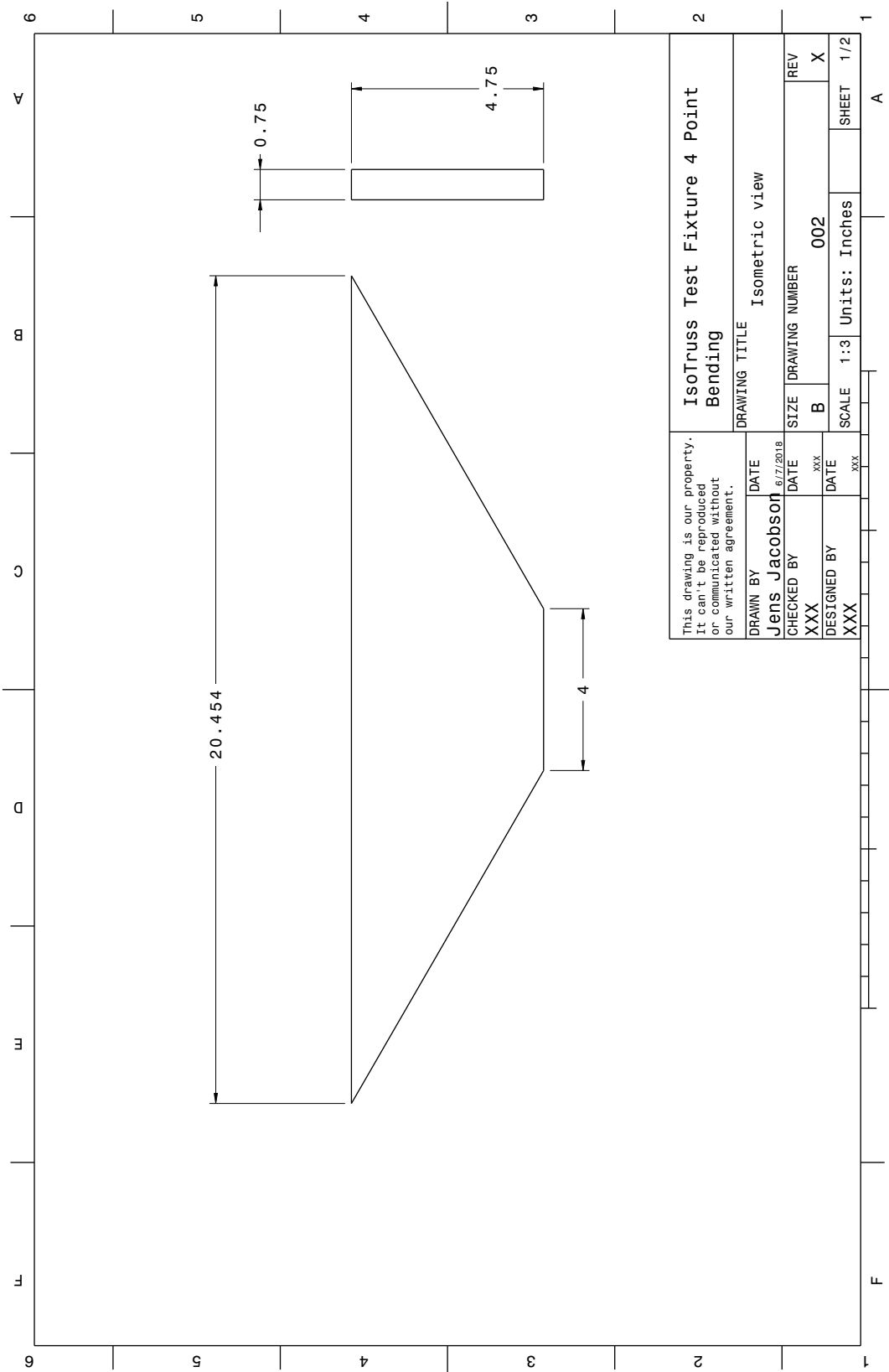


Figure A.8: Cure cycle for Specimen 13.

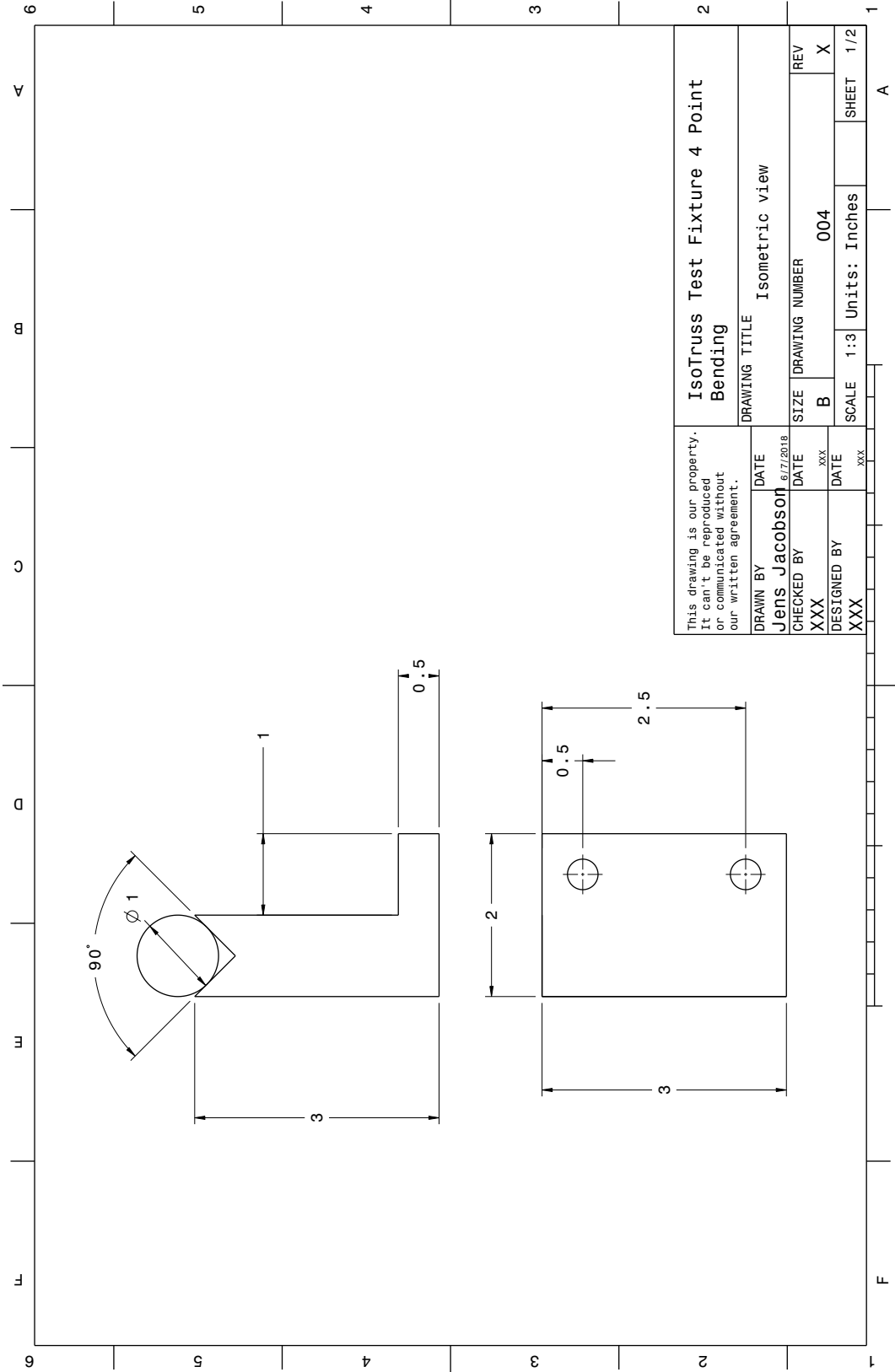
## A.4 Bending Fixture Drawings

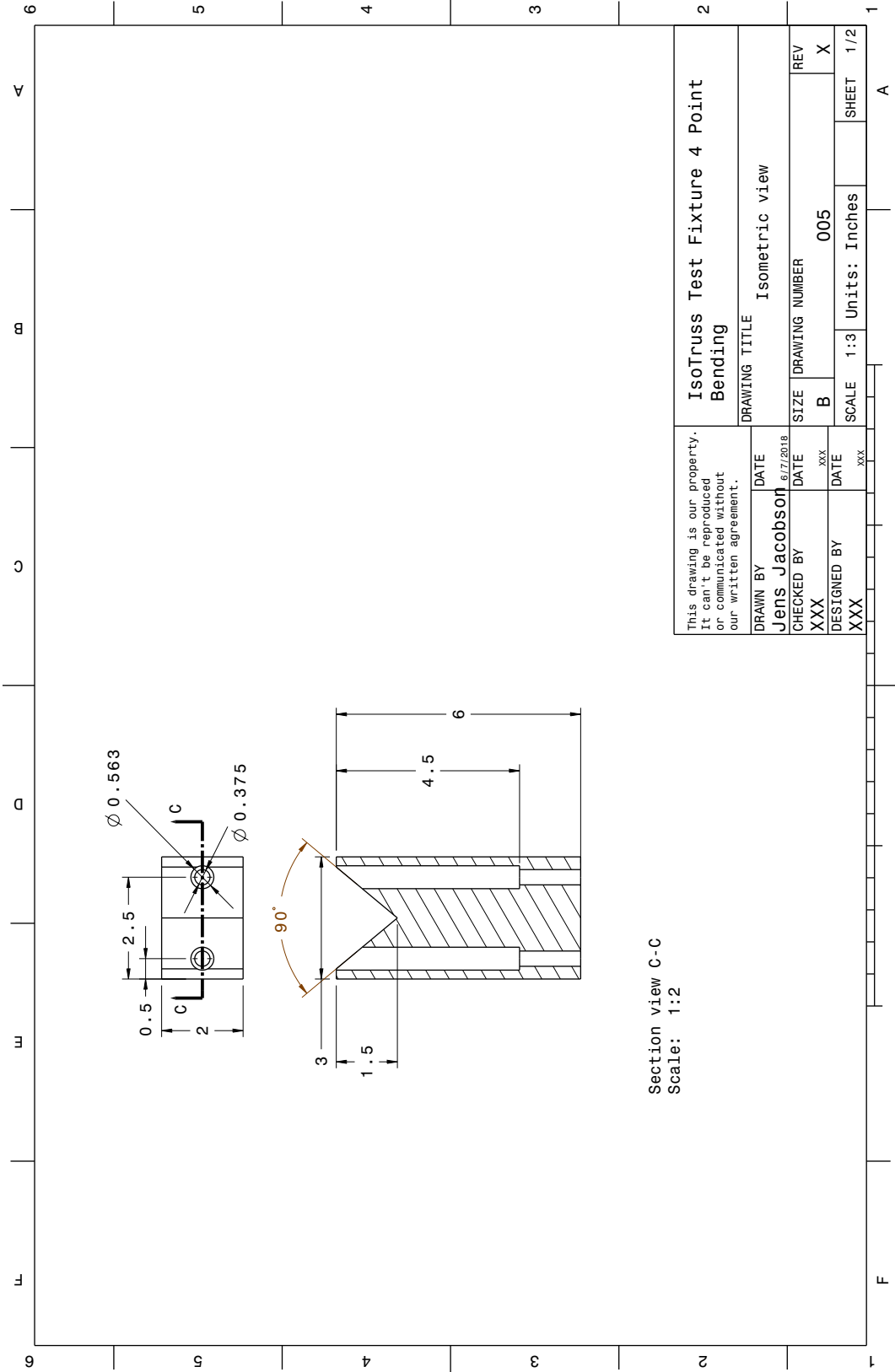


This drawing is our property. It can't be reproduced or communicated without our written agreement.		DATE	6/7/2018
DRAWN BY	Jens Jacobson	DATE	xxx
CHECKED BY	xxx	DATE	xxx
DESIGNED BY	xxx	DATE	xxx
DRAWING TITLE		IsoMetric view	
IsoTruss Test Fixture 4 Point Bending		SIZE	B
DRAWING NUMBER		001	REV
SCALE		1:3	WEIGHT (kg)
4.82		SHEET	1/2



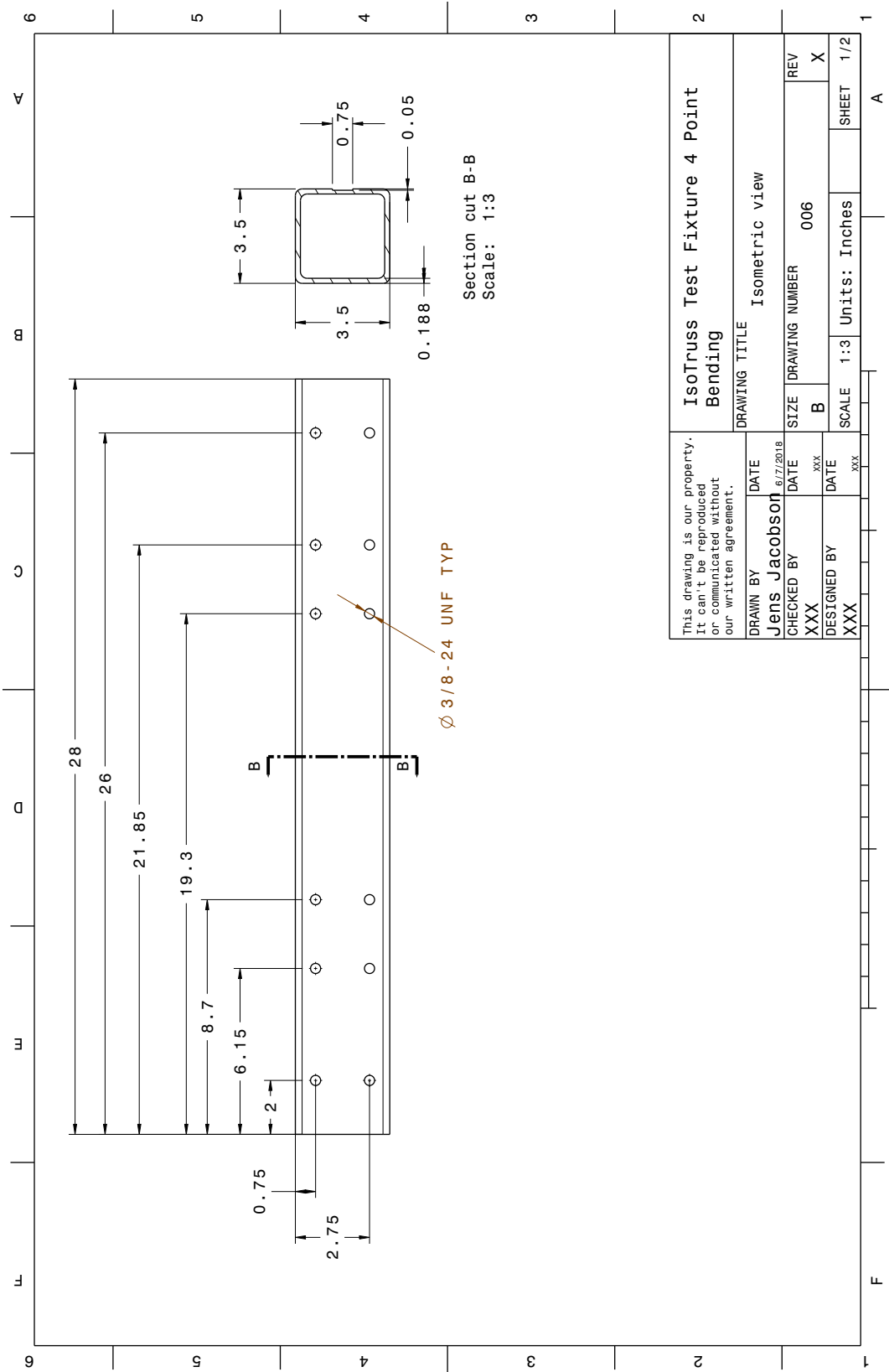
This drawing is our property. It can't be reproduced or communicated without our written agreement.		DRAWING TITLE		IsoTruss Test Fixture 4 Point Bending	
DRAWN BY	DATE	SIZE	DRAWING NUMBER	REV	
Jens Jacobson	6/7/2018	B	002	X	
CHECKED BY	DATE	SCALE	Units: Inches	SHEET	1/2
XXX	XXX	1:3			
DESIGNED BY	DATE				
XXX	XXX				

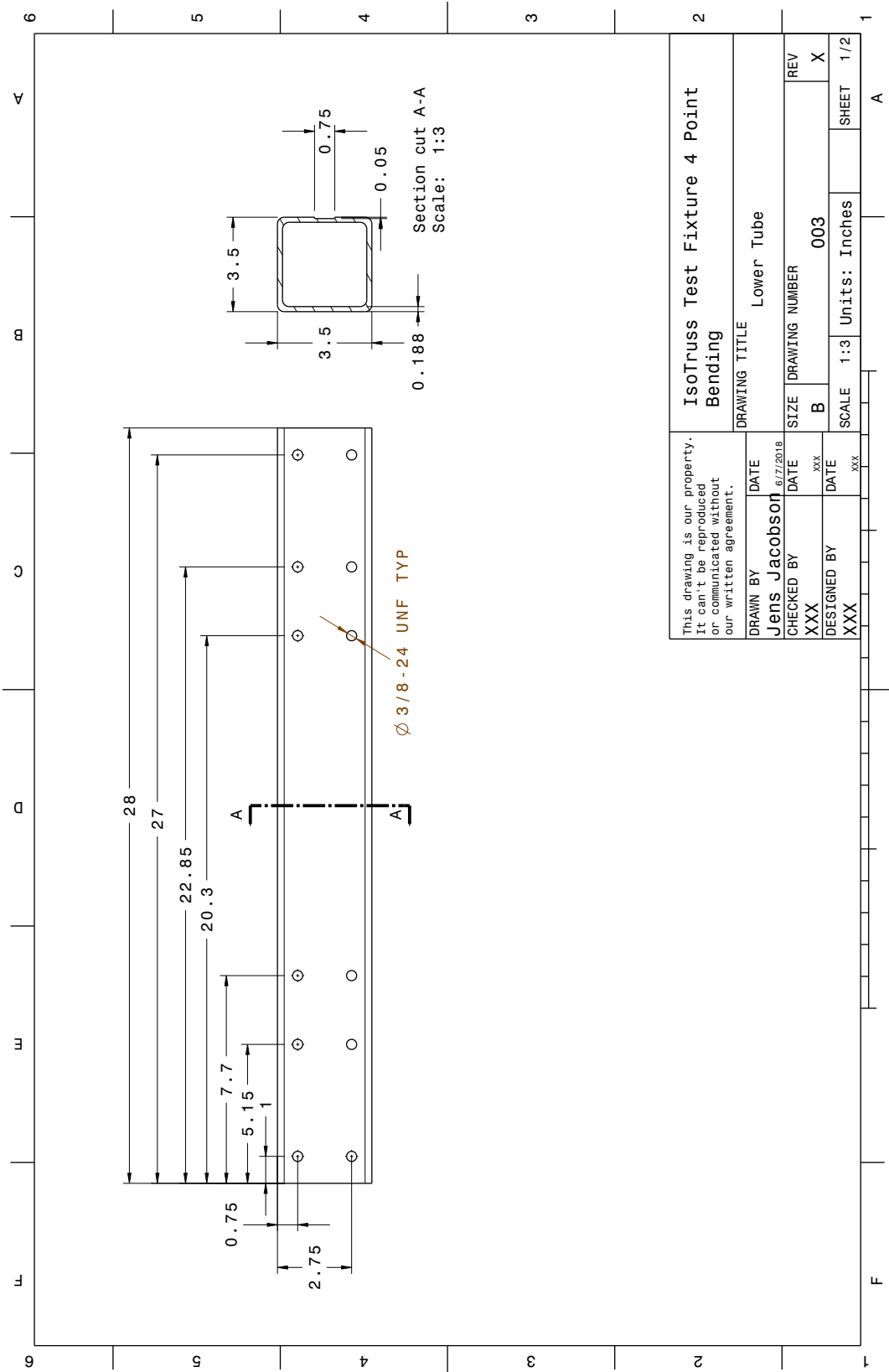




Section view C-C  
Scale: 1:2

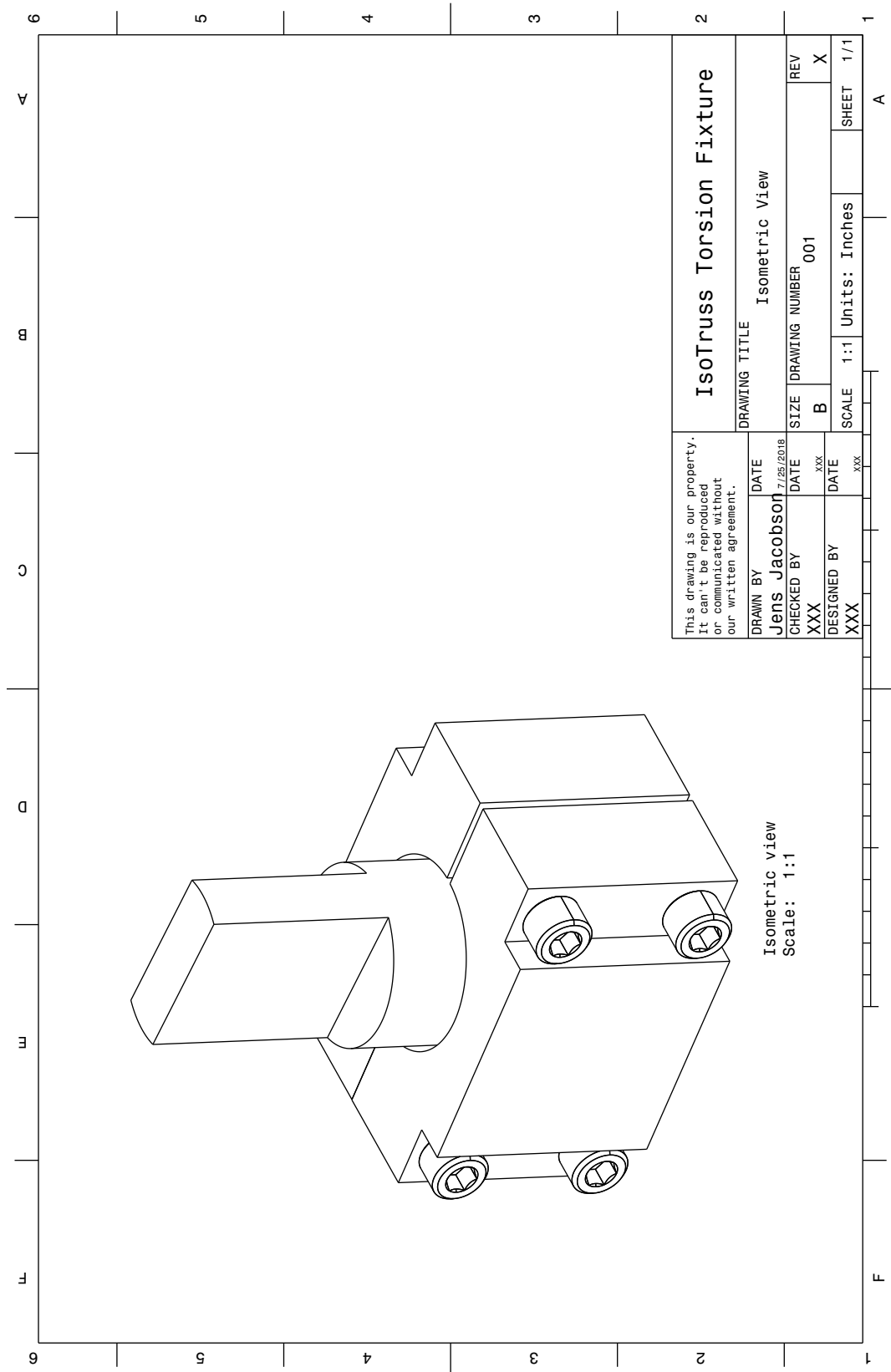
This drawing is our property. It can't be reproduced or communicated without our written agreement.		DRAWING TITLE		IsoTruss Test Fixture 4 Point Bending	
DRAWN BY	DATE	SIZE	DRAWING NUMBER	REV	
Jens Jacobson	6/7/2018	B	005	X	
CHECKED BY	DATE	SCALE	Units:	Inches	SHEET 1/2
XXX	XXX	1:3			A
DESIGNED BY	DATE				
XXX	XXX				

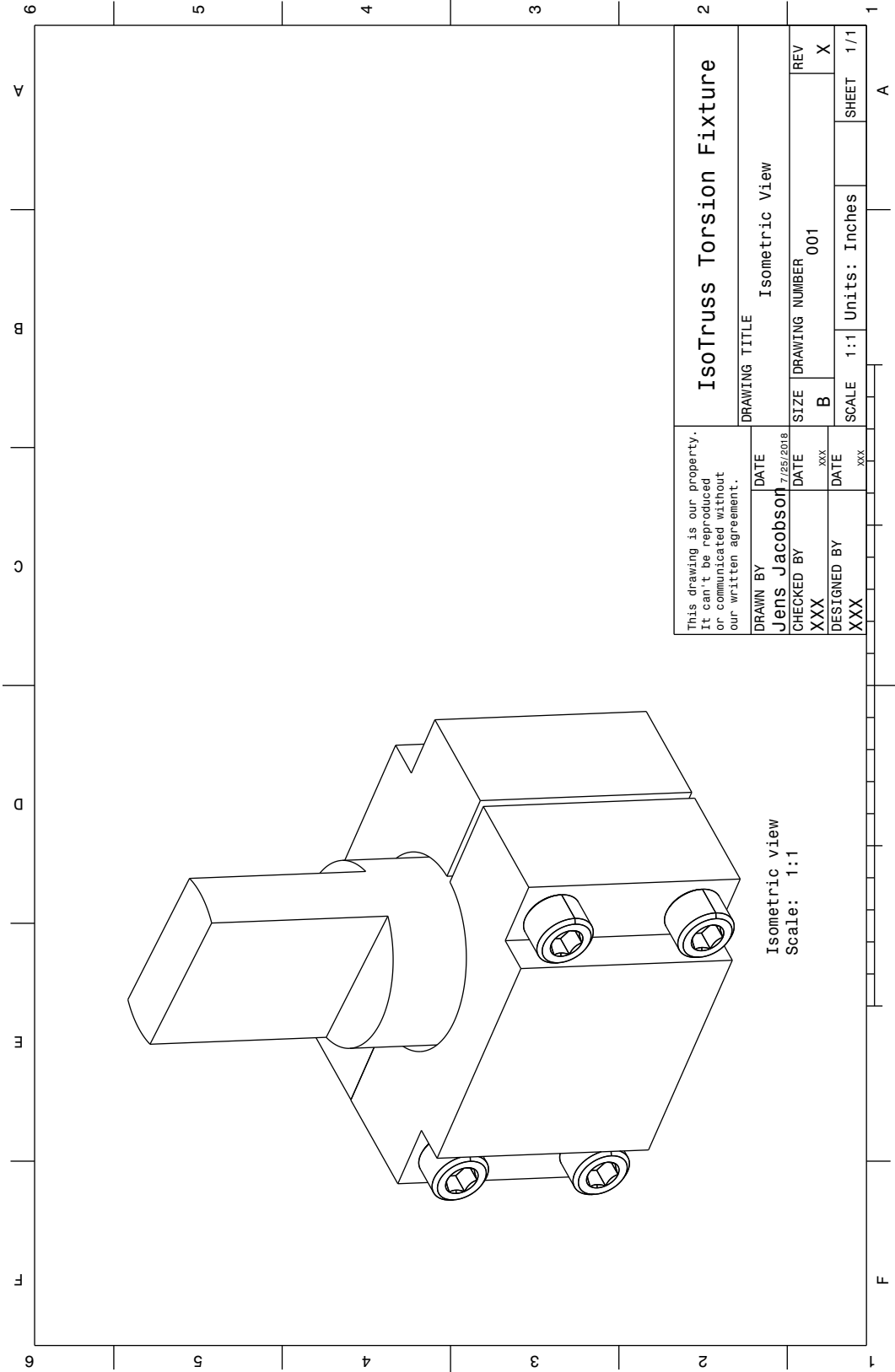






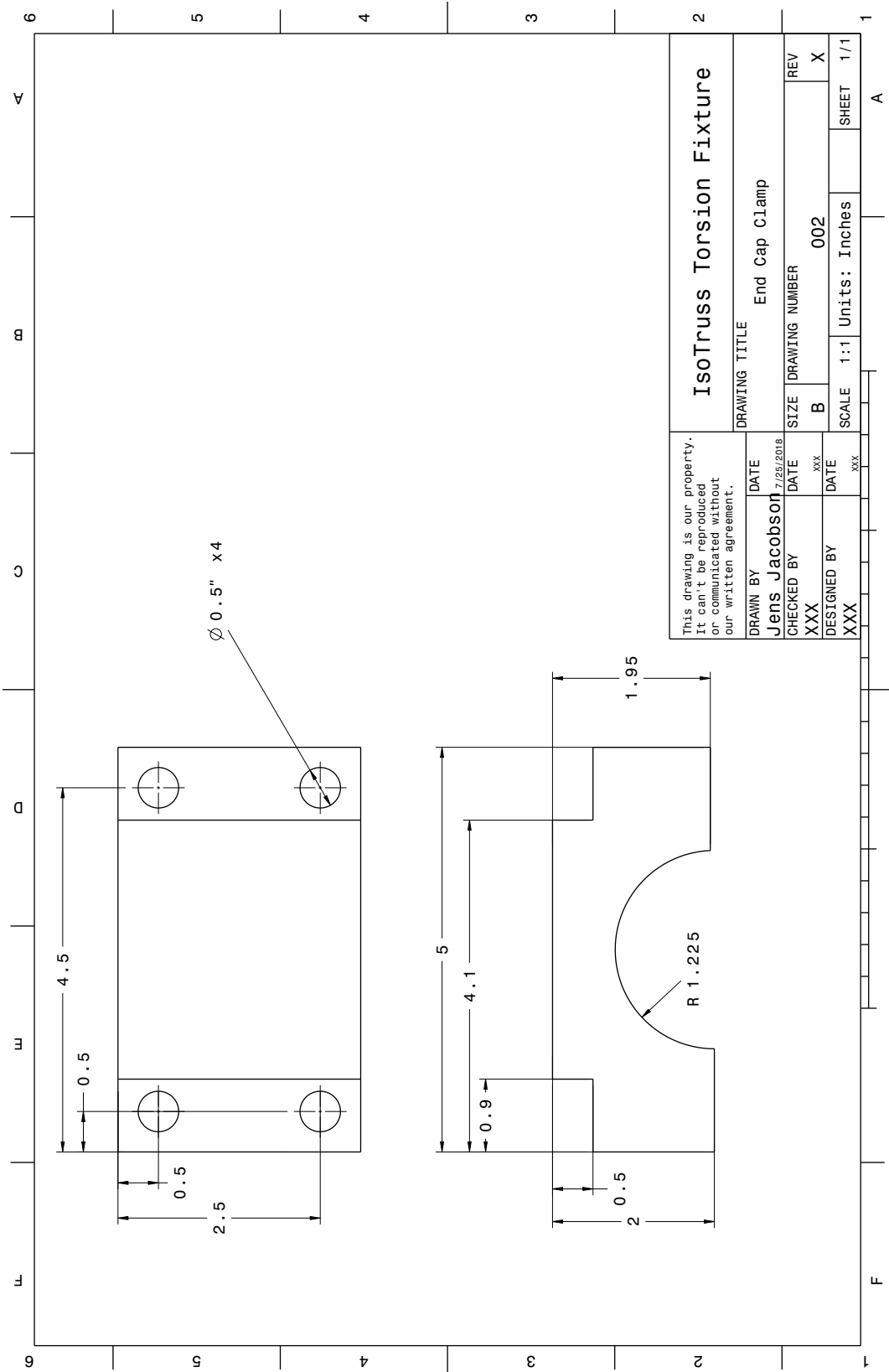
## A.5 Torsion Fixture Drawings

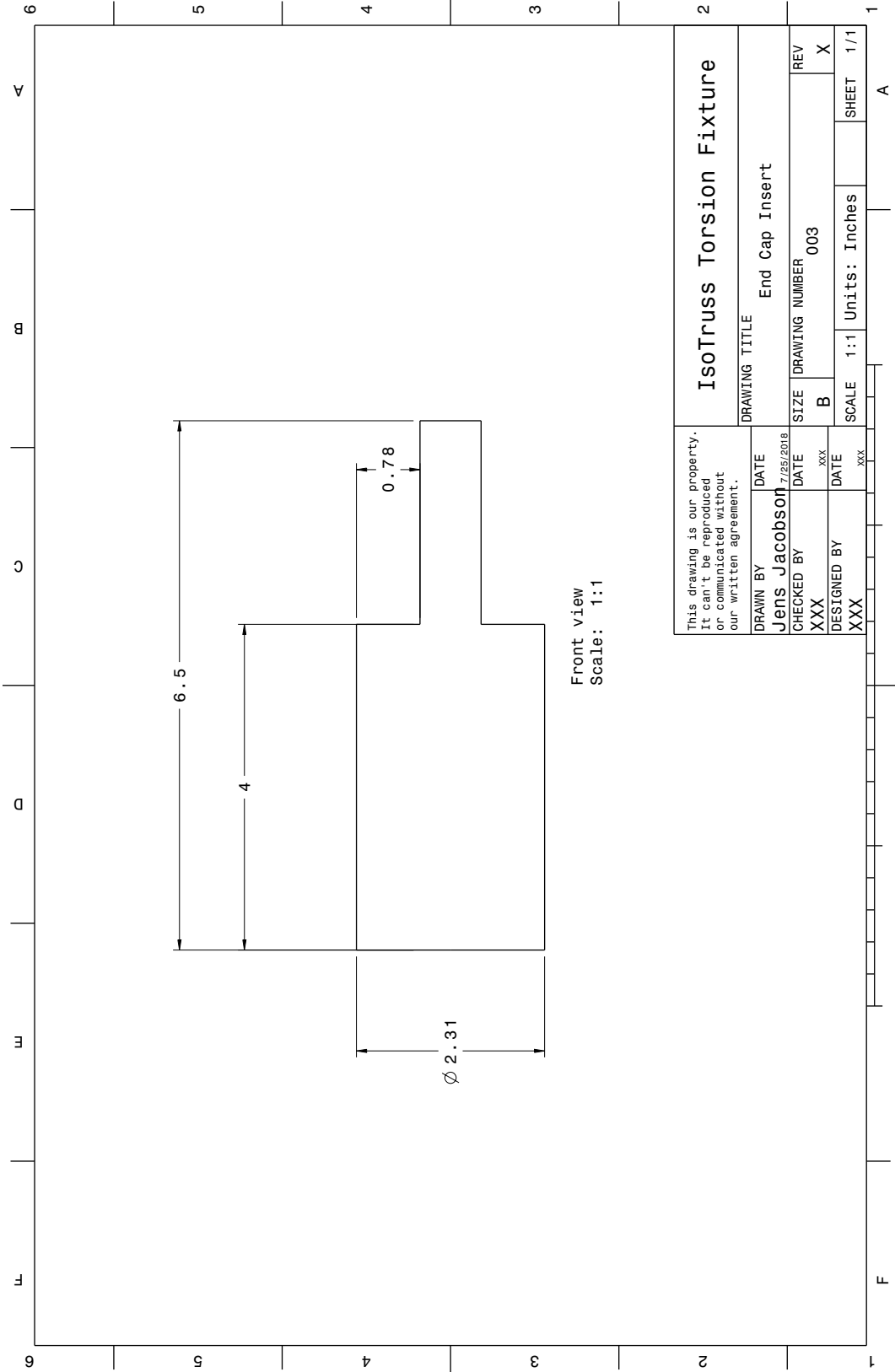




Isometric view  
Scale: 1:1

This drawing is our property. It can't be reproduced or communicated without our written agreement.		DATE	DRAWING TITLE	
DRAWN BY	Jens Jacobson	7/25/2018	IsoTruss Torsion Fixture	
CHECKED BY	XXX	DATE	SIZE	DRAWING NUMBER
DESIGNED BY	XXX	DATE	B	001
XXX	XXX	XXX	SCALE	1:1
			Units:	Inches
				SHEET 1/1





Front view  
Scale: 1:1

## APPENDIX B. RAW DATA PLOTS FROM TESTING

### B.1 Raw Data Graphs with Trend Lines

#### B.1.1 Torsion

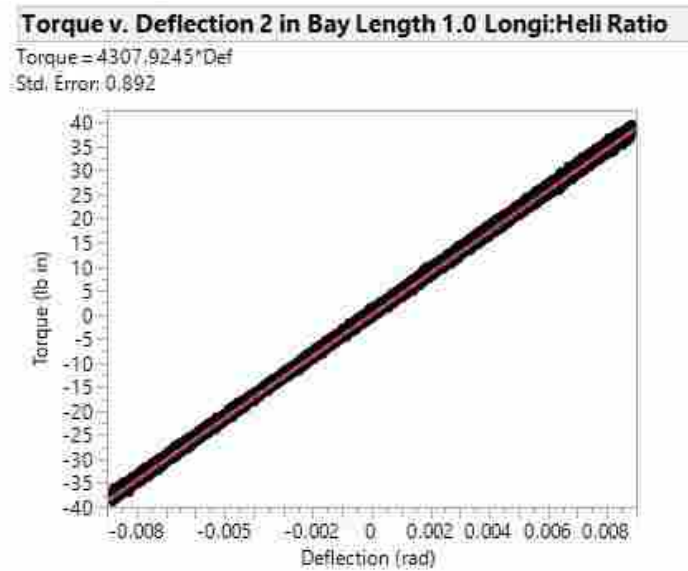


Figure B.1: Torque v. Rotation for 2 inch Bay Length, 1.0 Longitudinal to Helical Member ratio in torsion test

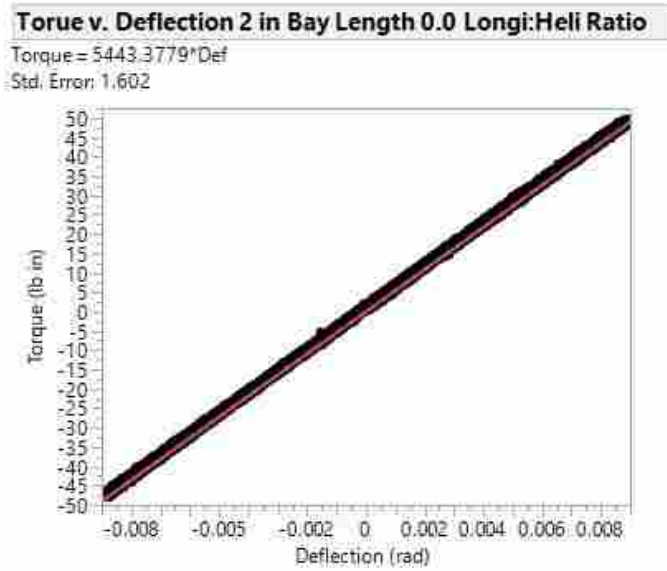


Figure B.2: Torque v. Rotation for 2 inch Bay Length, 0.0 Longitudinal to Helical Member ratio in torsion test

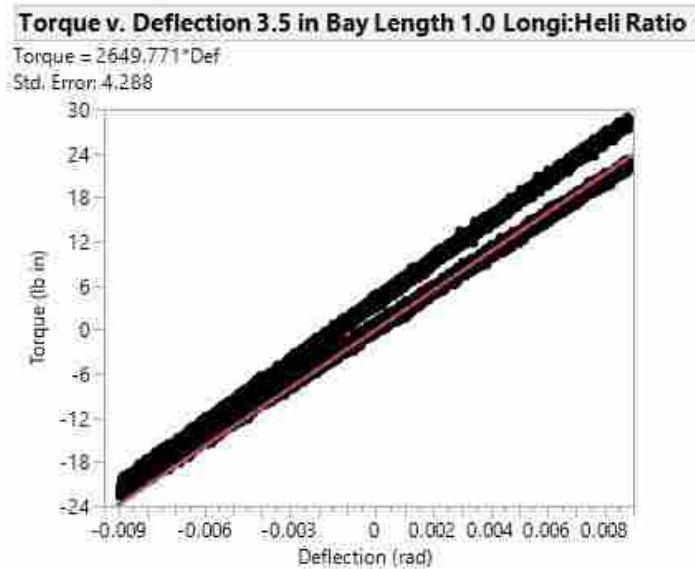


Figure B.3: Torque v. Rotation for 3.5 inch Bay Length, 1.0 Longitudinal to Helical Member ratio in torsion test

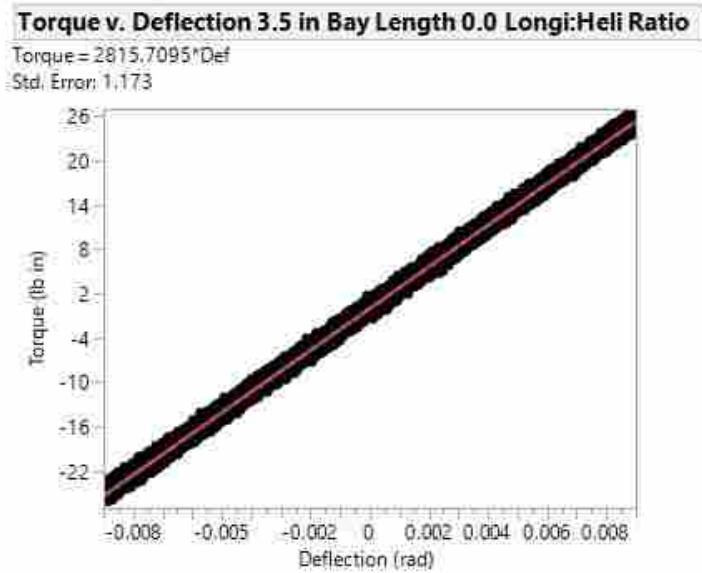


Figure B.4: Torque v. Rotation for 3.5 inch Bay Length, 0.0 Longitudinal to Helical Member ratio in torsion test

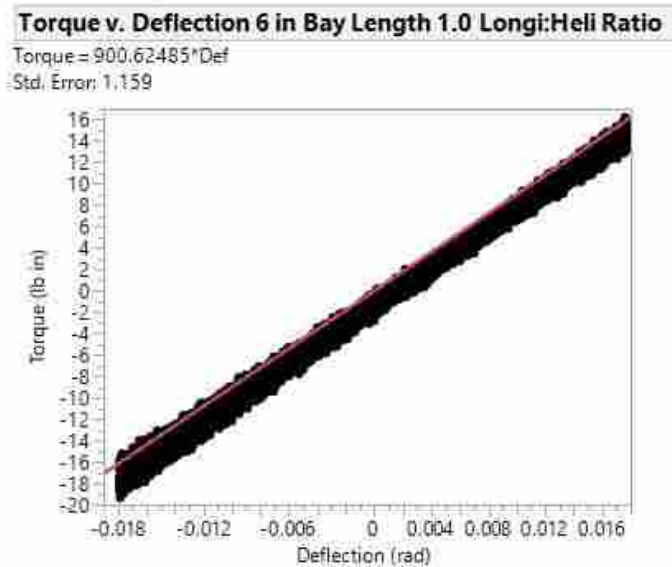


Figure B.5: Torque v. Rotation for 6 inch Bay Length, 1.0 Longitudinal to Helical Member ratio in torsion test

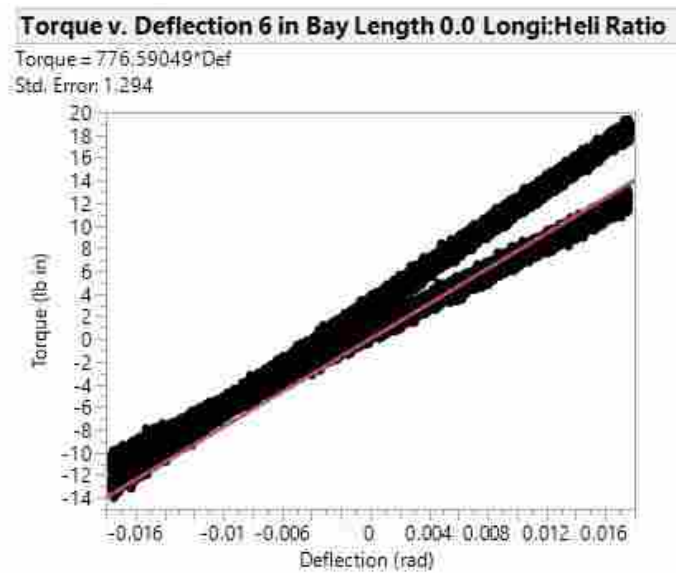


Figure B.6: Torque v. Rotation for 6 inch Bay Length, 0.0 Longitudinal to Helical Member ratio in torsion test



## APPENDIX C. FINITE ELEMENT ANALYSIS BATCH FILE

```
finish
/clear
! For building and analyzing an iso-truss
! Author: Jens Jacobson (Casey Tanner)
! 10_3_18
! The material properties used were collected from the data sheets for HexTow PV42/850
12K and for UF3323 epoxy resin. Shear modulus properties are estimated from Gibson 3rd edition
for similar modulus epoxy impregnated carbon fiber.
!Conversion factors:
fttoin = 12 ! converts
!*** Input Parameters:
key_long = 1 ! boolean, 0 to not include longitudinal members
Load_opt = 0 ! boolean, 0 for tip force, 1 for tip moment (both are displacement driven
loads) LHRatio = lh_rat ! Longitudinal to Helical Ratio (1/2 would indicate a 1:2 Longi:Heli)
*if,LHRatio,eq,0,then
key_long = 0
LHRatio = 1
*else
*endif
!GEOMETRY VARIABLES:
L = baylen ! in, length
Nb = 2 ! number of full bays along truss (minus 1 b/c of program indexing, Ex. 6 bays is
Nb = 5)
N = 6 ! num nodes around circumfrence of truss
```

$D1 = 4.6$   
 $D2 = \text{diatruess ! in, diameter from node to node (largest possible diameter measure)}$   
 $e\text{num} = 5$   
**! MATERIAL PROPERTIES:**  
 $E_{xx} = 29.95e6 \text{ ! psi, Young's Modulus in axial direction on each member}$   
 $G_{xy} = .671e6 \text{ ! adjust shear moduli for before/after break in period}$   
 $G_{xz} = .671e6$   
 $\text{Nu} = .3 \text{ ! Poisson's ratio}$   
 $\text{towards} = .00038$   
 $\text{helitownum} = 4$   
 $\text{heli\_area} = \text{towards} * \text{helitownum}$   
 $\text{heli\_dia} = \sqrt{4 * \text{heli\_area} / 3.141592}$   
 $\text{heli\_rad} = \text{heli\_dia} / 2$   
 $\text{longitownum} = \text{helitownum} * \text{LHRatio}$   
 $\text{longi\_area} = \text{towards} * \text{longitownum}$   
 $\text{longi\_dia} = \sqrt{4 * \text{longi\_area} / 3.141592}$   
 $\text{longi\_rad} = \text{longi\_dia} / 2$   
**!APPLIED LOADS**  
 $F_{\text{axial}} = 0 \text{ !lbs}$   
 $F_{\text{bend}} = 0 \text{ !lbs}$   
 $\text{tip\_angle} = 5 * 3.141592 / 180 \text{ ! Rad}$   
 $\text{torque} = 0 \text{ !in lbs (ftlbs *12)}$   
**!\*\*\* Math to get remaining geometric parameters:**  
 $\text{TH} = 360 / N \text{ ! degrees, figure 4 in 'IsoTruss Geometry 6.pdf'}$   
 $\text{THr} = \text{TH} * 3.14159 / 180 \text{ ! TH in radians}$   
 $c1 = \cos(\text{THr}) / (1 + \cos(\text{THr})) \text{ ! constant that defines l1 as a ratio of b}$   
 $b = L / (N * b1 + c1) \text{ ! length of each full bay}$   
 $R = D1 / 2 \text{ ! Nodal radius}$   
 $R_{\text{node}} = D2 / 2$   
 $h = \sqrt{b^2 + (D1^2) * (\sin(\text{THr})^2)} \text{ ! Node to Node length of helical member}$

```

delta1 = R*(cos(THr)/cos(THr/2)) ! See figure 4 in 'IsoTruss Geometry 6.pdf'
delta2 = R*cos(THr)*tan(THr/2)
delta3 = R*sin(THr)-delta2
l_1 = c1*b
!Manufacturing specific
R_pinrad = .25/2
TH_offset = atan(R_pinrad*2/(R_node-R_pinrad*2))/3.14159*180 heli_ang = atan(delta2/(l_1/2))
z_offset = R_pinrad*4/tan(heli_ang)
c2 = 1/(1+cos(THr)) ! constant that defines l2 as a ratio of b
l2 = c2*b ! See figure 4 in 'IsoTruss Geometry 6.pdf'
h1 = c1*h/2
h2 = c2*h/2
/prep7
csys,1 ! Cylindrical coordinates, (R,TH,Z), make sure you use TH in degrees
!*** ELEMENT TYPE
ET,1,BEAM188
ET,2,BEAM188
!MATERIAL PROP INPUT
MPTEMP,1,0
MPDATA,EX,1,,Exx
MPDATA,PRXY,1,,nu
MPDATA,GXY,1,,Gxy
MPDATA,GXZ,1,,Gxz
!Material Properties for the rigid bars where deflections are applied.
MPDATA,EX,2,,1e12
MPDATA,PRXY,2,,nu
MPDATA,GXY,2,,1e12
!Helical Cross Section
SECTYPE, 1, BEAM, CSOLID, circ, 0
SECOFFSET, CENT

```

```

SECDATA,heli_rad,
!Longitudinal Cross Section
SECTYPE, 2, BEAM, CSOLID, circ, 0
SECOFFSET, CENT
SECDATA,longi_rad,
!*** PLOTTING NODES
Nnodes = 0
Nanti = 0
Ntransi = 0
Ntot = 0
*DO,i,1,N,1
*DO,j,0,Nb,1
*if,j,eq,0,then
k,,R*cos(THr)/cos(THr/2)-.105,(i-.5)*TH,(j)*b !transition
Ntransi = Ntransi + 1
Ntot = Ntot + 1
k,,R*cos(THr)-.07,i*TH,(j)*b !anti-node
Nanti = Nanti + 1
Ntot = Ntot + 1
k,,R*cos(THr)/cos(THr/2),(i-.5)*TH,((j+c1/2)+(j+c1))/2*b
!transition
Ntransi = Ntransi + 1
Ntot = Ntot + 1
k,,R_node,i*TH,(j+1-c2/2)*b !node
k,,R_node-R_pinrad,i*TH+TH_offset,(j+1-c2/2)*b-z_offset
k,,R_node-R_pinrad,i*TH+TH_offset,(j+1-c2/2)*b+z_offset
k,,R_node-R_pinrad,i*TH-TH_offset,(j+1-c2/2)*b-z_offset
k,,R_node-R_pinrad,i*TH-TH_offset,(j+1-c2/2)*b+z_offset
Nnodes = Nnodes + 1
Ntot = Ntot + 1

```

```

*else
k,,R*cos(THr)/cos(THr/2),(i-.5)*TH,(j)*b !transition
Ntransi = Ntransi + 1
Ntot = Ntot + 1
k,,R*cos(THr),i*TH,(j+c1/2)*b !anti-node
Nanti = Nanti + 1
Ntot = Ntot + 1
k,,R*cos(THr)/cos(THr/2),(i-.5)*TH,(j+c1)*b !transition
Ntransi = Ntransi + 1
Ntot = Ntot + 1
k,,R_node,i*TH,(j+1-c2/2)*b !node
k,,R_node-R_pinrad,i*TH+TH_offset,(j+1-c2/2)*b-z_offset
k,,R_node-R_pinrad,i*TH+TH_offset,(j+1-c2/2)*b+z_offset
k,,R_node-R_pinrad,i*TH-TH_offset,(j+1-c2/2)*b-z_offset
k,,R_node-R_pinrad,i*TH-TH_offset,(j+1-c2/2)*b+z_offset
Nnodes = Nnodes + 1
Ntot = Ntot + 1
*endif
*ENDDO
*ENDDO
!*** Plotting last anti and transition nodes
*DO,i,1,N,1
!k,,R*cos(THr)/cos(THr/2),(i-.5)*TH,(Nb+1)*b
k,,R*cos(THr)/cos(THr/2),(i-.5)*TH,((Nb+1+c1/2)+(Nb+1))/2*b
Ntransi = Ntransi + 1
k,,R*cos(THr)-.07,i*TH,(Nb+1+c1)*b
Nanti = Nanti + 1
k,,R*cos(THr)/cos(THr/2)-.105,(i-.5)*TH,(Nb+1+c1)*b
Ntransi = Ntransi + 1
*ENDDO

```

```

!*** Plot helical lines
*DO,i,1,N,1
*DO,j,0,Nb+1,1
*if,j,eq,0,then
!!str,kp(R*cos(THr)/cos(THr/2),(i-.5)*TH,(j)*b),kp(R*cos(THr),i*TH,(j+c1/2)*b) !trans1
to anti
!!str,kp(R*cos(THr)/cos(THr/2),(i-.5)*TH,(j)*b),kp(R*cos(THr),(i)*TH,(j+c1/2)*b)
lstr,kp(R*cos(THr)-.07,i*TH,(j)*b),kp(R*cos(THr)/cos(THr/2),(i-.5)*TH,(j+c1/2)*b) !anti
to trans2
lstr,kp(R*cos(THr)-.07,i*TH,(j)*b),kp(R*cos(THr)/cos(THr/2),(i+.5)*TH,(j+c1/2)*b)
*elseif,j,eq,Nb+1,then
lstr,kp(R*cos(THr)/cos(THr/2),(i-.5)*TH,(j+c1/2)*b),kp(R*cos(THr)-.07,i*TH,(j+c1)*b) !trans1
to anti
lstr,kp(R*cos(THr)/cos(THr/2),(i+.5)*TH,(j+c1/2)*b),kp(R*cos(THr)-.07,i*TH,(j+c1)*b)
!!lstr,kp(R*cos(THr),i*TH,(j+c1/2)*b),kp(R*cos(THr)/cos(THr/2),(i-.5)*TH,(j+c1)*b) !anti
to trans2
!!lstr,kp(R*cos(THr),i*TH,(j+c1/2)*b),kp(R*cos(THr)/cos(THr/2),(i+.5)*TH,(j+c1)*b)
*else
lstr,kp(R*cos(THr)/cos(THr/2),(i-.5)*TH,(j)*b),kp(R*cos(THr),i*TH,(j+c1/2)*b) !trans1 to
anti
lstr,kp(R*cos(THr)/cos(THr/2),(i-.5)*TH,(j)*b),kp(R*cos(THr),(i-1)*TH,(j+c1/2)*b)
lstr,kp(R*cos(THr),i*TH,(j+c1/2)*b),kp(R*cos(THr)/cos(THr/2),(i-.5)*TH,(j+c1)*b) !anti
to trans2
lstr,kp(R*cos(THr),i*TH,(j+c1/2)*b),kp(R*cos(THr)/cos(THr/2),(i+.5)*TH,(j+c1)*b)
*endif
*if,j,eq,Nb+1,exit
lstr,kp(R*cos(THr)/cos(THr/2),(i-.5)*TH,(j+c1)*b),kp(R_node-R_pinrad,i*TH-TH_offset,(j+1-
c2/2)*b-z_offset) !trans2 to pre node
lstr,kp(R_node-R_pinrad,i*TH-TH_offset,(j+1-c2/2)*b-z_offset),kp(R_node,i*TH,(j+1-c2/2)*b)
!pre node to node

```

```

lstr,kp(R*cos(THr)/cos(THr/2),(i+.5)*TH,(j+c1)*b),kp(R_node-R_pinrad,i*TH+TH_offset,(j+1-
c2/2)*b-z_offset)
lstr,kp(R_node-R_pinrad,i*TH+TH_offset,(j+1-c2/2)*b-z_offset),kp(R_node,(i)*TH,(j+1-c2/2)*b)
lstr,kp(R_node,i*TH,(j+1-c2/2)*b),kp(R_node-R_pinrad,i*TH+TH_offset,(j+1-c2/2)*b+z_offset)
!node to pre node
lstr,kp(R_node-R_pinrad,i*TH-TH_offset,(j+1-c2/2)*b+z_offset),kp(R*cos(THr)/cos(THr/2),(i-
.5)*TH,(j+1)*b) !pre node to trans l
lstr,kp(R_node,i*TH,(j+1-c2/2)*b),kp(R_node-R_pinrad,i*TH-TH_offset,(j+1-c2/2)*b+z_offset)
lstr,kp(R_node-R_pinrad,i*TH+TH_offset,(j+1-c2/2)*b+z_offset),kp(R*cos(THr)/cos(THr/2),(i+.5)*TH,(j
*ENDDO
*ENDDO
!MESHING Helical Members
LATT,1,,,,,1 !Line Attribute- assigns cross-section and material to meshing
MSHAPE,0,2D !MeshShape- specifies quadrilateral (0,2D) or triangular (1,2D) or Hexahedral(6-
sided) (0,3D) or Tetrahedral(4-sided) (1,3D)
MSHKEY,1 !MeshKey- specifies free(0) or mapped(1)
LESIZE,ALL,,elnum, !Line Element Size- NL1(Number of Line or ALL),Size (Size of
Element if NDIV is blank), AngSize,NDIV (Number of Divisions)
LMESH,ALL !Line Mesh
!Deselect the helical lines to plot and mesh longitudinal lines
lsel,none
!*** Plot Longitudinal lines
*if,key_long,eq,1,then
*DO,i,1,N,1
*DO,j,0,Nb+1,1
*if,j,eq,0,then
lstr,kp(R*cos(THr)/cos(THr/2)-.105,(i-.5)*TH,(j)*b),kp(R*cos(THr)/cos(THr/2),(i-.5)*TH,(j+c1/2)*b)
*elseif,j,eq,Nb+1,then
lstr,kp(R*cos(THr)/cos(THr/2),(i-.5)*TH,(Nb+1+c1/2)*b),kp(R*cos(THr)/cos(THr/2)-.105,(i-
.5)*TH,(Nb+1+c1)*b)

```

```

*else
  !str,kp(R*cos(THr)/cos(THr/2),(i-.5)*TH,(j)*b),kp(R*cos(THr)/cos(THr/2),(i-.5)*TH,(j+c1)*b)
!trans1 to trans2
*endif
*if,j,eq,Nb+1,exit
  !str,kp(R*cos(THr)/cos(THr/2),(i-.5)*TH,(j+c1)*b),kp(R*cos(THr)/cos(THr/2),(i-.5)*TH,(j+1)*b)
!trans2 to trans1
*ENDDO
*ENDDO
!MESHING Longitudinal Members
LATT,1,,,,,2 !Line Attribute- assigns cross-section and material to meshing
MSHAPE,0,2D !MeshShape- specifies quadrilateral (0,2D) or triangular (1,2D) or Hexahedral(6-
sided) (0,3D) or Tetrahedral(4-sided) (1,3D)
MSHKEY,1 !MeshKey- specifies free(0) or mapped(1)
LESIZE,ALL,,,elnum, !Line Element Size- NL1(Number of Line or ALL),Size (Size of
Element if NDIV is blank), AngSize,NDIV (Number of Divisions)
LMESH,ALL !Line Mesh
*else
*endif
!sel,none
!Construct the rigid members at the end of the beam to provide a location to apply displace-
ments or loads
k,,0,0,L
*DO,i,1,N,1
*if,key_long,eq,1,then
  !str,kp(0,0,L),kp(R*cos(THr)-.07,(i)*TH,(Nb+1+c1)*b)
  !str,kp(0,0,L),kp(R*cos(THr)/cos(THr/2)-.105,(i-.5)*TH,(Nb+1+c1)*b)
*else
  !str,kp(0,0,L),kp(R*cos(THr)-.07,(i)*TH,(Nb+1+c1)*b)
*endif

```



```

*ENDDO
!Mesh the End Beam
LATT,2,,,,,1 !Line Attribute- assigns cross-section and material to meshing
MSHAPE,0,2D !MeshShape- specifies quadrilateral (0,2D) or triangular (1,2D) or Hexahedral(6-
sided) (0,3D) or Tetrahedral(4-sided) (1,3D)
MSHKEY,1 !MeshKey- specifies free(0) or mapped(1)
LESIZE,ALL,,enum, !Line Element Size- NL1(Number of Line or ALL),Size (Size of
Element if NDIV is blank), AngSize,NDIV (Number of Divisions)
LMESH,ALL !Line Mesh
!Reselect all lines
lsel,all
!BOUNDARY CONDITIONS AND LOADING
*DO,i,1,N,1
*if,key_long,eq,1,then
d,node(R*cos(THr)-.07,(i)*TH,0),ALL,0
d,node(R*cos(THr)/cos(THr/2)-.105,(i-.5)*TH,0),ALL,0
*else
d,node(R*cos(THr)-.107,(i)*TH,0),ALL,0
*endif
*ENDDO
!To do rotational displacement, replace rotx with rotz
d,node(0,0,L), ROTX,tip_angle
!Exit the preprocessor
fini
!Enter the solver
/SOL
NSUBST,30,70,5 !Specifies number of sub steps to be taken ( of substeps, Max , Min )
OUTRES,ERASE !Controls solution data written to database, ERASE resets to default
OUTRES,ALL,ALL !(Item, Freq)ALL, writes all data except LOCI and SVAR. ALL,
writes solution for every substep

```

```
TIME,1 !Sets time for a load step
solve
fini
/post1
/SHRINK,0
/ESHAPE,1.0
/EFACET,1
/RATIO,1,1,1
/CFORMAT,32,0
/EDGE,1,0,45
/GLINE,1,-1
/VIEW,1,1
/ANG,1
/REP,FAST
/dscale,1,1 !Specifies plot scale
pldi,1 !Plots deformed shape
nselect,s,loc,z,L !Selects nodes at the end of the truss
PRRSOL,MX !Outputs MX, or the bending moment for this case
ALLSEL,ALL
```

## APPENDIX D. DERIVATION OF DEFLECTION OF A SIMPLY SUPPORTED BEAM WITH ECCENTRIC LOAD

A simplified depiction of the load case is seen in Figure D.1.

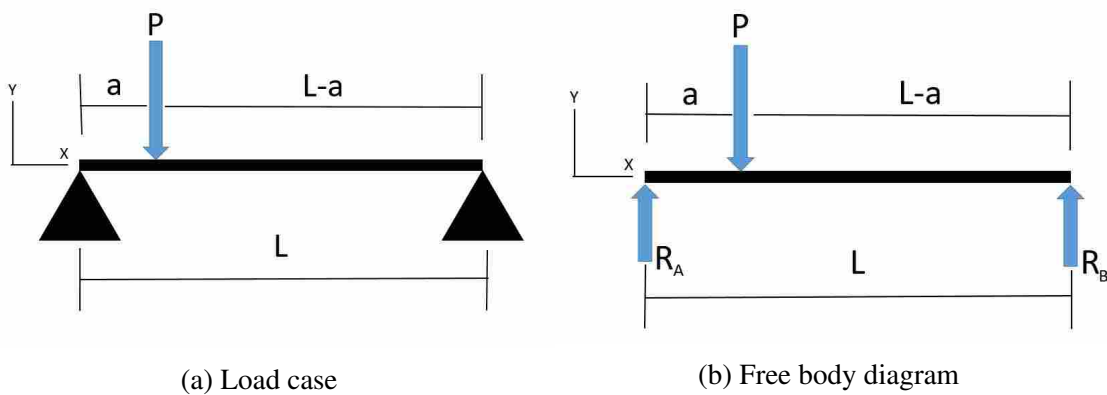


Figure D.1: Eccentric load applied to a simply supported beam.

Solving the equilibrium equations for the reaction forces:

$$\Sigma F_y = 0 \tag{D.1}$$

$$0 = R_A + R_B - P \tag{D.2}$$

$$\Sigma M_A = 0 \tag{D.3}$$

$$0 = -Pa + R_B L \tag{D.4}$$

$$R_B = \frac{Pa}{L} \tag{D.5}$$

Substitute D.5 into D.2:

$$R_A = \frac{P(L-a)}{L} \tag{D.6}$$

The internal moment to the left of the point load:

$$M = \frac{Px(L-a)}{L} \quad (\text{D.7})$$

The internal moment to the right of the point load:

$$M = -P(x-a) + \frac{Px(L-a)}{L} \quad (\text{D.8})$$

Introducing the differential equation for elastic curvature [10]:

$$\frac{d^2y}{dx^2} = -\frac{M}{EI} \quad (\text{D.9})$$

Substituting D.7 into D.9 and integrating:

$$\frac{dy}{dx} = \frac{1}{EI} \int \frac{Px(L-a)}{L} dx \quad (\text{D.10})$$

$$\frac{dy}{dx} = \frac{1}{EI} \left( \frac{Px^2(L-a)}{2L} + C_1 \right) \quad (\text{D.11})$$

$$y = \frac{1}{EI} \int \frac{Px^2(L-a)}{2L} + C_1 dx \quad (\text{D.12})$$

$$y = \frac{1}{EI} \left( \frac{Px^3(L-a)}{6L} + C_1x + D_1 \right) \quad (\text{D.13})$$

Substituting D.8 into D.9 and integrating:

$$\frac{dy}{dx} = \frac{1}{EI} \int -P(x-a) + \frac{Px(L-a)}{L} dx \quad (\text{D.14})$$

$$\frac{dy}{dx} = \frac{1}{EI} \left( \frac{-P(x-a)^2}{2} + \frac{Px^2(L-a)}{2L} + C_2 \right) \quad (\text{D.15})$$

$$y = \frac{1}{EI} \int \frac{-P(x-a)^2}{2} + \frac{Px^2(L-a)}{2L} + C_2 dx \quad (\text{D.16})$$

$$y = \frac{1}{EI} \left( \frac{-P(x-a)^3}{6} + \frac{Px^3(L-a)}{6L} + C_2x + D_2 \right) \quad (\text{D.17})$$

Introducing boundary conditions:

Table D.1: Boundary Conditions

Case 1	Case 2	Case 3	Case 4
$x = 0$	$x = L$	$x = a$	$x = 0$
$y = 0$	$y = 0$	$y_{Left} = y_{Right}$	$y'_{Left} = y'_{Right}$

Case 1, use Equation D.13 and BC case 1:

$$0 = \frac{1}{EI} \left( \frac{P(0)^3(L-a)}{6L} + C_1(0) + D_1 \right) \quad (\text{D.18})$$

$$D_1 = 0 \quad (\text{D.19})$$

Case 2, use Equation D.17 and BC case 2:

$$0 = \frac{1}{EI} \left( \frac{-P(L-a)^3}{6} + \frac{PL^3(L-a)}{6L} + C_2L + D_2 \right) \quad (\text{D.20})$$

Case 3, use Equations D.13, D.17, and D.19 with BC case 3:

$$\frac{1}{EI} \left( \frac{Pa^3(L-a)}{6L} + C_1a \right) = \frac{1}{EI} \left( \frac{-P(a-a)^3}{6} + \frac{Px^3(L-a)}{6L} + C_2a + D_2 \right) \quad (\text{D.21})$$

$$\frac{Pa^3(L-a)}{6L} + C_1a = \frac{Pa^3(L-a)}{6L} + C_2a + D_2 \quad (\text{D.22})$$

$$\frac{Pa^3(L-a)}{6L} - \frac{Pa^3(L-a)}{6L} = C_2a - C_1a + D_2 \quad (\text{D.23})$$

$$(C_2 - C_1)a + D_2 = 0 \quad (\text{D.24})$$

Case 4, use Equations D.11 and D.15 with BC case 4:

$$\frac{1}{EI} \left( \frac{Pa^2(L-a)}{2L} + C_1 \right) = \frac{1}{EI} \left( \frac{-P(a-a)^2}{2} + \frac{Pa^2(L-a)}{2L} + C_2 \right) \quad (\text{D.25})$$

$$\frac{Pa^2(L-a)}{2L} + C_1 = \frac{Pa^2(L-a)}{2L} + C_2 \quad (\text{D.26})$$

$$\frac{Pa^2(L-a)}{2L} - \frac{Pa^2(L-a)}{2L} = C_2 - C_1 \quad (\text{D.27})$$

$$C_2 - C_1 = 0 \quad (\text{D.28})$$

Substitute Equation D.28 into D.24:

$$D_2 = 0 \quad (\text{D.29})$$

Substitute Equation D.29 into D.20:

$$0 = \frac{1}{EI} \left( \frac{-P(L-a)^3}{6} + \frac{PL^3(L-a)}{6L} + C_2L \right) \quad (\text{D.30})$$

$$C_2L = \frac{P(L-a)^3}{6} - \frac{PL^3(L-a)}{6L} \quad (\text{D.31})$$

$$C_2 = \frac{P(L-a)^3}{6L} - \frac{PL(L-a)}{6} \quad (\text{D.32})$$

Substitute Equation D.32 with D.29 into D.17:

$$y = \frac{1}{EI} \left( \frac{-P(x-a)^3}{6} + \frac{Px^3(L-a)}{6L} + \left( \frac{P(L-a)^3}{6L} - \frac{PL(L-a)}{6} \right) x + 0 \right) \quad (\text{D.33})$$

$$y = \frac{1}{EI} \left( \frac{-P(x-a)^3}{6} + \frac{Px^3(L-a)}{6L} + \frac{Px(L-a)^3 - PxL^2(L-a)}{6L} \right) \quad (\text{D.34})$$

$$y = \frac{-P(x-a)^3}{6EI} + \frac{Px^3(L-a)}{6EIL} + \frac{Px}{6EIL} ((L-a)^3 - L^2(L-a)) \quad (\text{D.35})$$

$$y = \frac{-P(x-a)^3}{6EI} + \frac{Px^3(L-a)}{6EIL} + \frac{Px}{6EIL} (L^3 - 3L^2a + 3La^2 - a^3 - L^3 + L^2a) \quad (\text{D.36})$$

$$y = \frac{-P(x-a)^3}{6EI} + \frac{Px^3(L-a)}{6EIL} - \frac{Pax}{6EIL} (2L^2 - 3La + a^2) \quad (\text{D.37})$$

$$y = \frac{-P(x-a)^3}{6EI} + \frac{Px^3(L-a)}{6EIL} - \frac{Pax}{6EIL} (2L-a)(L-a) \quad (\text{D.38})$$

If  $y = \delta_{\frac{L}{2}}$ :

$$\delta_{\frac{L}{2}} = -\frac{Pa}{6EIL} (2L-a)(L-a) \left( \frac{L}{2} \right) + \frac{P(L-a)}{6EIL} \left( \frac{L}{2} \right)^3 - \frac{P}{6EI} \left( \frac{L}{2} - a \right)^3 \quad (\text{D.39})$$

Solving for EI to calculate the flexural rigidity:

$$EI = -\frac{Pa}{6\delta_{\frac{L}{2}}L}(2L-a)(L-a)\left(\frac{L}{2}\right) + \frac{P(L-a)}{6\delta_{\frac{L}{2}}L}\left(\frac{L}{2}\right)^3 - \frac{P}{6\delta_{\frac{L}{2}}}\left(\frac{L}{2}-a\right)^3 \quad (\text{D.40})$$